



Climate sensitivity and geomorphological response of cirque glaciers from the late glacial to the Holocene, Sierra Nevada, Spain

David Palacios ^{a,*}, Marc Oliva ^b, Antonio Gómez-Ortiz ^b, Nuria Andrés ^a, José M. Fernández-Fernández ^c, Irene Schimmelpfennig ^d, Laëticia Léanni ^d, A.S.T.E.R. Team ^{d,e}

^a Department of Geography, Universidad Complutense de Madrid, Madrid, Spain

^b Department of Geography, Universitat de Barcelona, Barcelona, Spain

^c Instituto de Geografia e Ordenamento do Território, Universidade de Lisboa, Lisboa, Portugal

^d Aix Marseille Université, CNRS, IRD, INRAE, Coll. France, CEREGE, Aix-en-Provence, France

^e Consortium: Georges Aumaître, Didier Bourlès, Karim Keddadouche, France

ARTICLE INFO

Article history:

Received 4 June 2020

Received in revised form

11 September 2020

Accepted 23 September 2020

Available online 30 September 2020

Keywords:

Glacial cirque

Rock glacier

Sierra Nevada

Cosmic-ray exposure dating

Late glacial

Holocene

ABSTRACT

Through a detailed geomorphological study, including thorough mapping of the geomorphic features as well as ¹⁰Be Cosmic-Ray Exposure (CRE) dating, the geomorphological evolution of the Mulhacén cirque since the maximum ice extent of the last glacial cycle until nowadays was determined. This glacial cirque is shaped on the northern face of the Mulhacén peak (3479 m a.s.l. 37°03'12"N/3°18'41"W), Sierra Nevada, southern Spain. It includes several depositional and erosional glacial landforms that allowed reconstructing its environmental evolution since the last glacial cycle. Furthermore, the sequence of glacial oscillations from this site was compared to that of other cirques of the massif, evidencing that: (i) new glaciers formed in these cirques during the Younger Dryas (YD), and (ii) disappeared at 11.7 ± 1.0 ka. Depending on the altitude, orientation and height of the cirque walls, the final deglaciation of the cirques generated a diversity of landscapes, including a wide range of glacial and periglacial landforms, such as polished surfaces, sequences of moraines, proto-rock glaciers or large rock glacier systems. No glaciers existed in the Sierra Nevada during the Middle Holocene. Only the cirques whose summits exceed 3300 m, are north-exposed and whose walls exceed 300 m high (i.e. Mulhacén and Veleta) hosted glaciers during Neoglacial phases, including the Little Ice Age (LIA) (approx. 1300–1850 CE). During these periods, climate oscillations favoured the formation of small glaciers in these cirques, which generated large moraine systems with either one polygenic ridge or a sequence of spaced frontal arcs. The existence of glaciers impeded the formation of permafrost-related landforms, such as rock glaciers and protalus lobes until the end of the LIA, when they started to form. These results are compared with the deglacial evolution in 55 cirques from Iberian mountains as well as from glacial cirques from other mid-latitude mountains and subpolar regions. The chronology of their deglaciation as well as the landforms generated during glacial retreat followed similar patterns, with no significant differences at regional scale. For each mountain range, the geomorphological diversity existing in each cirque depends on the local topographic characteristics although they formed during the same climatic phases.

© 2020 Elsevier Ltd. All rights reserved.

1. Introduction

Glacial cirques are defined as armchair-shaped erosional hollows, typified by steep headwalls, typically arcuate and with lateral spurs, and with overdeepened floors, often occupied by a lake or

bog (Evans and Cox, 1974, 1995; Barr and Spagnolo, 2015). The typology of cirques is extremely diversified and, therefore, the limits of this concept are difficult to define (Mindrescu and Evans, 2014). Their origin is associated with the first steps of glaciation (Benn and Evans, 2010), although the mechanisms involved in their formation and upgrowth are still under debate (Sanders et al., 2012, 2013). Since the first studies, the importance of palaeoclimatic conditions driving the glacial and periglacial processes that shaped the heads

* Corresponding author.

E-mail address: davidp@ucm.es (D. Palacios).

of the valleys is highlighted (Benedict, 1973; Delmas et al., 2015; Barr et al., 2017). Consequently, several parameters such as the distribution, aspect, floor elevation and morphometry of the glacial cirques have been used to infer palaeotemperatures, precipitation gradients, cloud-cover and prevailing wind directions during glaciation (e.g. Dahl and Nesje, 1992; Barr and Spagnolo, 2015; Ipsen et al., 2018). However, other factors such as the geological structure, post-glacial erosion and the uncertainty regarding their origin make even more challenging to reconstruct past climate regimes using cirque morphometry (Barr and Spagnolo, 2015).

Moreover, it must be taken into account that enhanced by paraglacial dynamics, glacial cirques continue in many cases to evolve during the interglacial periods following the last phase of glaciation (Kleman and Stroeven, 1997; Ballantyne, 2002, 2013). This is especially important in the mountain ranges under Mediterranean influence, where glacial cirques are one of the most abundant glacial landforms, affected by the last glacial cycle and subsequent deglaciation (Hughes et al., 2006, 2007). Over recent decades, in particular two palaeoenvironmental techniques, namely lake sediment record studies and Cosmic-Ray Exposure (CRE) dating of glacial landforms using cosmogenic nuclides, have provided evidence of the potential palaeoclimatic information preserved in alpine cirques.

Many mountain glaciers reached their maximum extent between 26.5 and 19 ka (Clark et al., 2009) or a few thousand years before (Hughes et al., 2013). This period is the so-called Last Glacial Maximum (LGM), which coincided with the minimum sea level at global scale (Clark et al., 2009; Hughes et al., 2013). However, this maximum extension was reached before or after the LGM in many other mountains, which is known as the Local Last Glacial Maximum (LLGM). In the Mediterranean region, particular attention has been paid to the reconstruction of the sequence of glacial phases recorded on cirque floors in the form of moraine systems revealing either (i) phases of stabilization during the long-term retreat since the LLGM, or (ii) short periods of glacial readvance. This is the case in the Rila mountains, Balkan Peninsula, where 2 km-long cirques include a large number of moraines that formed between the LGM and the Younger Dryas (YD) (12.9–11.7 ka, Walker et al., 2009; GS-1 Rasmussen et al., 2014), i.e. within the approx. 24–12 ka period (Kuhlemann et al., 2013). One of the best examples of the geomorphological interest of these small glacial cirques comes from Mount Olympus, southern Balkan Peninsula, where moraines from the Late Glacial to the latest Neoglacial advances (from 15.6 ± 2.0 to 0.64 ± 0.08 ka) are distributed over a distance of less than 500 m (Styllas et al., 2018). Similarly, in the Dinaric mountains, Žebre et al. (2019) summarized previous studies of numerous small cirques with a sequence of moraine systems dating back from Oldest Dryas (OD) to the YD (14.9 ka to 11.7 ka). Small cirques in the Apennines also retain geomorphic evidence in the form of moraine arcs formed between the LLGM and present-day (Giraudi, 2012; Baroni et al., 2018). There are many other examples of the potential of small cirques, including information about glacial oscillations occurred during Termination-1 (19–11.7 ka), such as in the Anatolian peninsula. Here, in Mount Geyikdag (Sarikaya et al., 2017) and Mount Uludag (Zahno et al., 2010), ca. 1 km long cirques contain moraines from the LLGM to the Holocene. A similar pattern is found in small cirques of the High Atlas, Morocco, with moraine systems from different phases encompassing the entire deglaciation until the early Holocene (Hughes et al., 2019).

Small glacial cirques with rich palaeoclimatic information are not exclusive of the Mediterranean region. Cirques are also frequent glacial features in continental ranges as, for example, those in Central Europe. Similar glacial chronologies as those described

above have been reported from cirques in the Krkonoše Mountains, Sudetes range (Engel et al., 2014), or in cirques of larger formerly glaciated ranges, such as the Tatra Mountains, Northern Carpathians (Engel et al., 2015; Makos et al., 2018; Zasadni et al., 2020), and Parang Mountains, Southern Carpathians (Gheorghiu et al., 2015), where moraines from the OD to the Holocene have been dated. Small cirques in the Alps also provided detailed information on glacial oscillations and the climatic evolution of the Late Holocene (Ribolini et al., 2007; Ivy-Ochs et al., 2009; Hippolyte et al., 2009; Moran et al., 2016; Ivy-Ochs, 2015; Le Roy et al., 2017). Well-known glacial oscillations from the last glacial phases in many cirques of several mountain ranges of the Western United States confirming previous results obtained in certain ranges such as the Sierra Nevada (Clark and Gillespie, 1997) have been recently published (Marcott et al., 2019; Laabs et al., 2020).

Glacial cirques in mountains that protruded from ice-sheet surfaces, such as those in nunataks, also include geomorphic evidence of glacial fluctuations during the last glacial cycle. This is the case of the Macgillycuddy's Reeks (South Ireland), where small cirques host moraines from the LLGM and even younger (Barth et al., 2016). Moreover, glacial cirques can also preserve accurate data on the last deglaciation phases of ice-sheets, as well as on Neoglacial advances during the current interglacial. For example, up to four glacial advances that occurred after the complete disappearance of the Scandinavian Ice-sheet have been evidenced in numerous cirques in Norwegian mountains (Dahl and Nesje, 1992; Paasche et al., 2007). In Svalbard, small cirques contain moraines revealing that the YD was only a minor advance, smaller than those of the Little Ice Age (from 1300 to about 1850 CE, LIA) (Mangerud and Landvik, 2007). One of the best examples of the palaeoclimatic significance of these cirques can be found in the Tröllaskagi Peninsula, northern Iceland, formerly covered by the Icelandic Ice-Sheet (Ipsen et al., 2018). In this peninsula, small cirques a few km long host up to 12 Holocene moraine complexes corresponding to various stages of the LIA, and even different glacial advances over the last decades (Fernández-Fernández et al., 2019). Moreover, other cirques in the Tröllaskagi Peninsula include a set of erratic boulders, moraines, and several generations of rock glaciers and debris-covered glaciers showing a complex glacial evolution from the OD to the present (Tanarro et al., 2019; Fernández-Fernández et al., 2020).

In the Iberian Peninsula, small glacial cirques including several moraine systems have been studied in the highest mountain ranges (Oliva et al., 2019). In the Eastern Pyrenees, very small cirques preserve erratic boulders, complex moraine systems and rock glaciers that reveal a complex glacial evolution from the LLGM to the Holocene (Pallàs et al., 2006, 2010; Delmas, 2015; Andrés et al., 2019; Jomelli et al., 2020). In the Central Pyrenees, small cirques include moraine complexes from the OD to the Holocene (Delmas, 2015; Palacios et al., 2017a; Crest et al., 2017; Tomkins et al., 2018), with only a few sites recording Neoglacial advances (García-Ruiz et al., 2014). In the Cantabrian Mountains, the heads of some cirques host rock glaciers and moraines from the OD to the Early Holocene (Rodríguez-Rodríguez et al., 2016, 2017). In the Iberian Range, cirques <1 km long preserved moraines from the LLGM, OD and remnants of fossil debris-covered glaciers, some of which were active until the Middle-Holocene due to their favourable orientation (Fernández-Fernández et al., 2017). Other cirques contain moraines from the LLGM to the OD, when the formation of rock glaciers occurs, and even subsequent deglaciated cirque steps, coetaneous with the YD (García-Ruiz et al., 2020a). In the Central Range, small cirques in the massifs of Guadarrama (Palacios and MarcosVázquez-Selem, 2011, 2012a; 2012b; Carrasco et al., 2016) and Gredos (Domínguez-Villar et al., 2013; Carrasco et al., 2013,

2015) include moraine complexes from the LLGM to the OD, YD and even the Holocene, depending on the altitude and prevailing aspect of the cirques. Besides, a detailed study of the peatbogs from a glacial cirque in Gredos has provided valuable palaeoclimatic information from the deglaciation from the OD to the present (López-Sáez et al., 2020).

The Sierra Nevada (South Iberia) contains 65 glacial cirques with geomorphic evidence indicative of the glacial and palaeoclimatic evolution from the LLGM to the recent times (Palacios et al., 2016; Palma et al., 2017) and, in some of these cirques, even from the previous glacial cycle (Palacios et al., 2019). Regarding the Holocene, several palaeoenvironmental archives such as lake records and peatbogs inside glacial cirques testify to a remarkable climatic variability (Oliva, 2009; Oliva and Gómez-Ortiz, 2012), as well as the impact of human activity (Anderson et al., 2011; García-Alix et al., 2013, 2017). Two of these cirques held also small glaciers during the LIA, which were the southernmost in Europe (Gómez-Ortiz et al., 2009, 2015, 2018). One of them, the Veleta cirque, shaped on the northern slope of the Veleta peak, contains valuable information on environmental dynamics from the first glacial phases of the LIA to the present-day, with evidence of: (i) the succession of several glacial advances and the gradual melting of the glacier, (ii) rock avalanches, (iii) landslides and, (iv) permafrost degradation. These processes, highly sensitive to small climatic variations, led to intense geomorphic readjustments typical of the paraglacial phase (Oliva et al., 2016; Palacios et al., 2019; Serrano et al., 2018; Gómez-Ortiz et al., 2019 and references therein). As a result, landforms from this cirque are considered key geoindicators for monitoring the impact of climate change on mountain geomorphological processes in southern Europe (Gómez-Ortiz et al., 2019). The other cirque that hosted a glacier during the LIA in the Sierra Nevada is located under the northern rock wall of Mulhacén peak. To date, although it contains a wide range of glacial depositional and erosional features, this cirque has been little studied. The only palaeoclimatic records from this cirque are those provided by the sediments of La Mosca Lake, which led to a detailed picture of the Mid-Late Holocene palaeoecological evolution as well as to the evidence of several glacial advances during the Late Holocene (Manzano et al., 2019; Oliva, 2009; Oliva et al., 2019).

On the other hand, the interpretation of the palaeoenvironmental records preserved in the interior of glacial cirques can come up against important difficulties, such as the alteration of glacial reliefs depending on the intensity of slope processes and the frequency of rock avalanches altering glacial landforms (Deline et al., 2015; Mercier et al., 2017; Knight et al., 2018) or the effects of neotectonic activity in cirque evolution (Oskin and Burbank, 2005). Regarding CRE dating, these processes can hinder the presumed undisturbed exposure of bedrock surfaces, rock glacier and moraine boulders to be dated, or potentially lead to nuclide inheritance in these surfaces (Li et al., 2016; Çiner et al., 2017; Köse et al., 2019). Therefore, the current state of knowledge still presents some open questions, such as:

- (i) What is the origin of the complex moraine formations frequently found inside the cirques and covering a wide chronological range?
- (ii) Why do glaciers, once confined within the cirques, tend to evolve in many different ways, forming, in some cases, debris-covered glaciers or rock glaciers, and, in other cases, multiple moraine ridges developing in short periods of time?
- (iii) Is it possible to circumvent the impact of geomorphological processes occurring inside the glacial cirques to correctly extract the palaeoenvironmental significance preserved in their records?

In order to address these questions, the glacial landforms existing in one of the Mediterranean cirques housing the most detailed sequence of the environmental evolution since the LLGM, the Mulhacén cirque, have been analysed. To investigate the potential common behaviour and infer its palaeoclimatic implications on different spatial scales, the palaeoclimatic and geomorphological evolution of this cirque is compared to that of others in the whole massif of Sierra Nevada, the Iberian Peninsula and other mountains of the Northern Hemisphere for which geomorphological and CRE data are available.

2. Study area

Located in the southern fringe of Iberia at latitude of 37°N, the Sierra Nevada is the highest massif of the Betic Range (Fig. 1). It includes the highest peaks in western Europe outside the Alps, with elevations exceeding 3000 m a.s.l. in its western fringe, such as Mulhacén (3479 m, 37°03'12"N 3°18'41"W) and Veleta (3396 m, 37°03'22"N, 3°21'56"W). The landscape of the massif results from its bordering location between different climatic influences: continental (Europe/Africa), maritime (Atlantic/Mediterranean) and subtropical high pressure belt/mid-latitude westerlies (Oliva et al., 2011). Currently, the mean annual air temperature at 2500 m is 4.4 °C (1965–1992), whereas at the highest summits of the massif at 3400 it is 0 °C (2001–2016) (Gómez-Ortiz et al., 2019). Annual precipitation reaches 710 mm, mostly as snow between October and April (Oliva, 2009; Oliva et al., 2008). The bedrock of the summit area, the study site, is composed of micaschists which are intensely affected by periglacial processes. The vegetation cover is very sparse, typical of the high semi-arid Mediterranean mountains, and is mostly distributed across the valley floors near lakes and wetlands (Oliva et al., 2011).

The contemporary landscape of the Sierra Nevada is mostly a consequence of past glaciations. A wide range of depositional and erosional landforms of glacial origin are distributed in elevations above 2000 (northern slopes) and 2500 m (southern slopes). They result from the sequence of glacial phases that shaped the highest lands of the massif since the maximum ice extent of the penultimate glacial cycle (Palacios et al., 2019). The LIA was the last period with the presence of glaciers in the Sierra Nevada (Gómez-Ortiz et al., 2009, 2012; 2015, 2018; Palacios et al., 2016).

The deglaciation of the cirques favoured the appearance of many mountain lakes and bogs which have been sampled for palaeoenvironmental and palaeoclimatic purposes (Anderson et al., 2011; García-Alix et al., 2013, 2017; Jiménez-Moreno and Anderson, 2012; Oliva et al., 2011, 2010). At the northern foot of the Mulhacén peak, a glacial lake dammed by a moraine ridge is located next to the cirque mouth at 2892 m a.s.l.: the Mosca Lake (ca. 90 m wide, 160 m long, 1 ha, 3.2 m deep) (Oliva and Gómez-Ortiz, 2012) (Fig. 1). A sequence of recessional moraines is connected to the large talus cones generated by frost shattering from the steep northern rock wall of the Mulhacén peak, almost 400 m high. These moraines show multiple collapses and subsidence features (Fig. 1) which evidence the degradation of the small isolated permafrost patches still existing today in the massif (Oliva et al., 2018; Serrano et al., 2018). The large talus cones are also being affected by widespread debris flows transporting sediments downslope during the melting season or during extreme rainfall events in late summer and early autumn. At the foot of the Mulhacén rock wall, there are a few semi-permanent snow-patches as well as a proglacial lobe formed following the final deglaciation of the cirque (Fig. 2), which is also indicative of the existence of permafrost at this site (Serrano et al., 2018; Gómez-Ortiz et al., 2019).

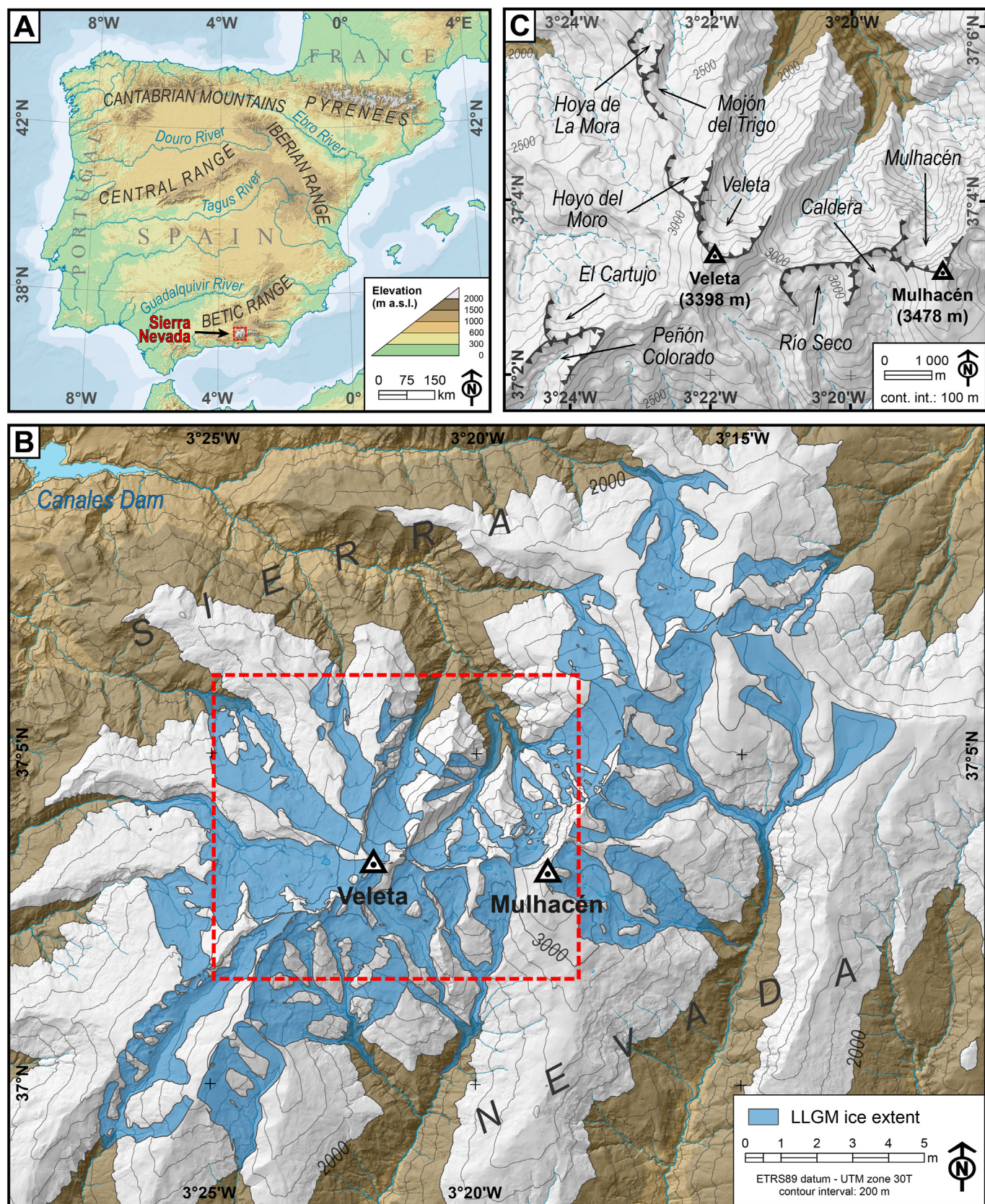


Fig. 1. Location map of the study area. A) Location of the Sierra Nevada in the context of the Iberian Peninsula. B) Glacier extent of the Sierra Nevada glaciers during their LLGM. C) Western sector of the Sierra Nevada where the main peaks and the cirques cited throughout the text are distributed.

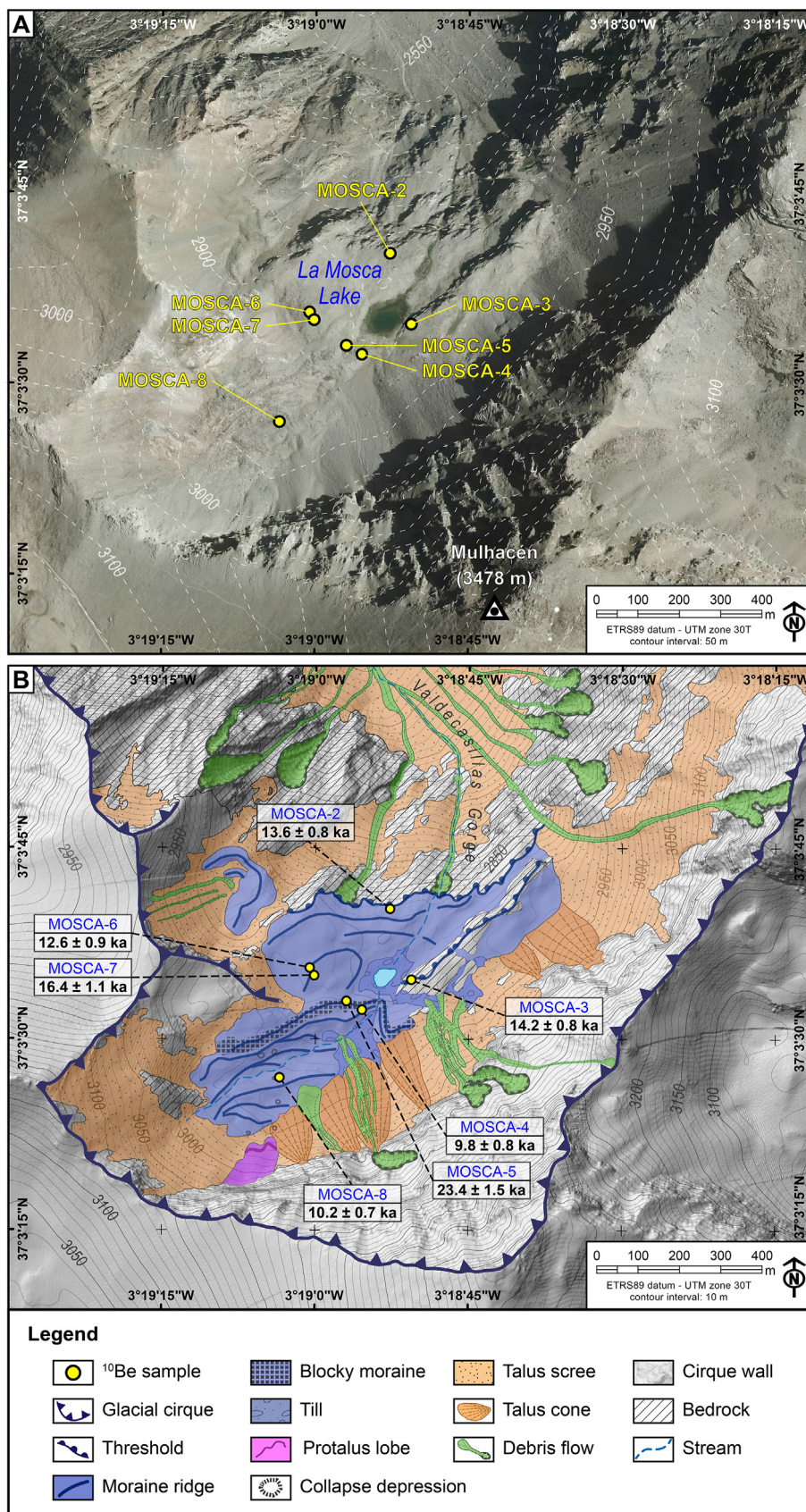


Fig. 2. Mulhacén cirque and location of the CRE sampling sites and ^{10}Be ages. A) Aerial orthophoto. B) Geomorphological map.

As revealed by historical documents and lacustrine sedimentary records, the cirque was partly glaciated several times during the Holocene, namely at 2.8–2.7, 1.4–1.2 and 0.51–0.24 ka cal BP (Oliva and Gómez-Ortiz, 2012; Oliva et al., 2020). Lake sediment phases recorded peaks with large concentrations of sand and very low organic carbon content, which are attributed to colder and wetter conditions and the development of a glacier in the catchment. The last of these periods coincided with the LIA, which promoted the formation of the largest glacier over the three last millennia in the Mulhacén cirque (Oliva and Gómez-Ortiz, 2012). There are other longer sedimentary cores collected from this lake with radiocarbon dates up to 8.4 cal ka BP, which however do not come from the basal sediments, but give a minimum age of lake formation following glacial retreat (Manzano et al., 2019). No chronological evidence is reported about earlier glacial phases. Therefore, the moraines located upstream of the La Mosca Lake have probably developed throughout the Holocene, whereas the moraines closing the lake must be older.

3. Methodology

3.1. Geomorphological mapping

In order to reconstruct the palaeoenvironmental evolution of the Mulhacén cirque since the last glacial cycle, a detailed geomorphological analysis and mapping of the study area was first performed. Although we consider the last glacial cycle as a synonymous of the Late Pleistocene (approx. 123–14 ka; Hughes and Gibbard, 2018), most of the preserved glacial landforms formed during the LGM or later. The different geomorphological units were classified following the criteria used in previous studies of other glacial cirques in this massif focusing on the distribution of moraines, rock glaciers, protalus lobes, rock avalanches, debris flows and rock falls (Gómez-Ortiz et al., 2012; Palacios et al., 2016; Palma et al., 2017). The spatial distribution of the different features of glacial origin revealed in this cirque suggests a sequence of glacial events until the recent disappearance of the LIA glacier. The geomorphological map was also used for planning the sampling strategy for CRE dating in order to establish the chronology of the cirque deglaciation. In addition, historical sources provided information concerning the periods during which glaciers were present during the LIA in the Sierra Nevada (Gómez-Ortiz et al., 2009, 2012, 2015, 2018). These were also used to interpret the final deglaciation phases of the Mulhacén cirque.

3.2. CRE sampling strategy

The sampling strategy for CRE dating is based on the sequence of the mapped landforms, from the bottom to the upper part of the cirque. In late summer 2016, when the cirque was snow-free and geomorphic features were clearly visible in the field, eight samples from the Mulhacén cirque at elevations between 2890 and 2950 m were collected. Two of the samples were taken from glacially polished outcrops (MOSCA-2 and MOSCA-3), while the others were taken from flat-topped surfaces of boulders located on moraine ridges. The characteristics of the sampling sites and complementary field data are summarized in Table 1.

3.3. CRE laboratory procedures and exposure age calculation

The samples were crushed and sieved to the 0.25–1 mm fraction at the 'Physical Geography Laboratory' of the Universidad Complutense de Madrid. The following steps of the sample preparation process were carried out at the 'Laboratoire National des Nucléides Cosmogéniques' (LN2C) of the CEREGE (Center Européen de Recherche et d'Enseignement des Géosciences de l'Environnement, Aix-en-Provence, France). To extract the cosmogenic ^{10}Be isotope, a first rough isolation of the quartz mineral fraction of the sieved samples was performed by means of a Frantz LB-1 magnetic separator removing the magnetic minerals. Subsequently, the remaining non-quartz minerals were dissolved through successive acid attacks (a mixture of concentrated hydrochloric (HCl) and hexafluorosilicic (H_2SiF_6) acids in a proportion 1:2). Three consecutive partial dissolutions using concentrated hydrofluoric acid (HF) were performed to ensure removal of any non-quartz mineral from the treated samples and to decontaminate the pure quartz mineral fraction from meteoric ^{10}Be . For the following steps, pure quartz masses ranged between 6 and 40 g 150 μL of an accurately weighted ^9Be carrier solution manufactured in-house from a phenakite crystal ($[^9\text{Be}] = 3025 \pm 9 \mu\text{g g}^{-1}$; Merchel et al., 2008) were added, and the quartz was totally dissolved in 48% HF (3.6 mL per g of quartz + 30 mL in excess). After the total dissolution, the resulting solution was evaporated until dryness and the solid residues were recovered in 7.1 M HCl. Samples were precipitated with ammonia before successive separations, first through an anion exchange column (Dowex 1 \times 8) to remove iron, and then through one or several cation exchange columns (Dowex 50WX8) to discard boron (isobar) and to separate the Be from other elements (Merchel and Herpers, 1999). All samples contained a lot of muscovite, which was difficult to remove completely and complicated the treatment of some of the samples. Therefore 17 cation exchange columns were

Table 1
Field data of sampling sites, topographic shielding factor, sample thickness and distance from the headwall.

Sample name	Sample type	Latitude (DD)	Longitude (DD)	Elevation (m a.s.l.)	Topographic shielding factor	Thickness (cm)	Distance from the headwall (m): map vs ground length
MOSCA-2	Polished outcrop	37.06117	−3.31463	2929	0.9757	3.0	904/1058
MOSCA-3	Polished outcrop	37.05963	−3.31405	2960	0.9545	2.0	911/1049
MOSCA-4	Moraine boulder	37.05897	−3.31539	2946	0.9579	2.5	886/1034
MOSCA-5	Moraine boulder	37.05916	−3.31581	2951	0.9579	2.5	932/1071
MOSCA-6	Moraine boulder	37.05989	−3.31681	2964	0.9572	3.0	1077/1194
MOSCA-7	Moraine boulder	37.05972	−3.31669	2962	0.9579	4.0	1050/1170
MOSCA-8	Moraine boulder	37.05749	−3.31763	2984	0.9460	4.0	706/862

performed for samples MOSCA-2, 3, 5 and 7.

The eluted Be was precipitated to beryllium hydroxide ($\text{Be}(\text{OH})_2$) with ammonia and oxidized to BeO at 700 °C. As a final step, BeO were mixed with niobium powder in an approximate 1:1 proportion, and then loaded in cathodes for the subsequent measurement of the $^{10}\text{Be}/^9\text{Be}$ ratio at the ASTER ('Accélérateur pour les Sciences de la Terre, Environnement et Risques') AMS (Accelerator Mass Spectrometry) national facility at CEREGE. A chemical blank was prepared along with the seven samples.

Sample $^{10}\text{Be}/^9\text{Be}$ ratios were calibrated against the in-house standard STD-11, using an assigned $^{10}\text{Be}/^9\text{Be}$ nominal ratio of $(1.191 \pm 0.013) \times 10^{-11}$ (Braucher et al., 2015).

Analytical 1σ uncertainties include uncertainties associated with AMS counting statistics, the standard $^{10}\text{Be}/^9\text{Be}$ ratio, an external AMS error of 0.5% (Arnold et al., 2010) and the chemical blank measurement. A ^{10}Be half-life of $(1.387 \pm 0.0012) \times 10^6$ years was used (Chmeleff et al., 2010; Korschinek et al., 2010). More details of analytical data are given in Table 1.

^{10}Be surface CRE ages were calculated using the CREp online calculator (Martin et al., 2017; available online at: <http://crep.crgp.cnrs-nancy.fr/#/>). The parameters used were: the LSD elevation latitude scaling scheme (Lifton et al., 2014), the ERA40 atmospheric model (Uppala et al., 2005) and the geomagnetic database based on the LSD framework (Lifton et al., 2014). This setting yielded a sea-level high latitude (SLHL) ^{10}Be production rate of 3.98 ± 0.22 atoms $\text{g}^{-1} \text{yr}^{-1}$. Rock density was assumed to be 2.7 g cm^{-3} . Partial shielding of the surrounding topography from the cosmic-ray flux was calculated through the Topographic Shielding Calculator v.2 of CRONUS-Earth Web Calculators (consulted 2020). CRE ages are reported for the zero denudation scenario, and uncertainties included hereafter include analytical and production rate errors (Table 2).

The results of the analysis carried out in the Mulhacén cirque have been confronted with previous studies involving CRE dating, some using ^{10}Be and others ^{36}Cl , conducted in other cirques of the Sierra Nevada and in the rest of the Iberian mountains. In order to compare the results obtained from the two cosmogenic nuclides, all the CRE ages mentioned in the text were recalculated in accordance with the protocols proposed for the Iberian Peninsula in Oliva et al. (2019). Also, to compare our results with those obtained in cirques from other mountains outside Iberian Peninsula where CRE dating was performed, we have checked all the publications of the last five years that include a detailed description of the CRE age calculation protocols and only those with similar protocols to those applied to Iberian mountains were considered.

In addition, the information on the glacial chronological sequences provided by the new CRE ages were compared with the palaeoenvironmental evidences previously inferred from the sedimentary studies of La Mosca Lake (Oliva and Gómez-Ortiz, 2012; Manzano et al., 2019) as well as from other lakes and peat-bogs of the massif (Anderson et al., 2011; García-Alix et al., 2013, 2017; Jiménez-Moreno and Anderson, 2012; Oliva et al., 2011, 2010).

4. Results

4.1. Geomorphological setting and CRE sample selection

The results of the geomorphological analysis of the Mulhacén cirque are summarized in the geomorphological map (Fig. 2) as well as along a transect including the most remarkable glacial and periglacial features (Fig. 3).

For CRE dating, we focused on rocky outcrops with glacially polished surfaces that protrude above the bottom of the cirque and had probably not been covered with sediment after deglaciation; however, few suitable sites were found as debris cover is very abundant in the Mulhacén cirque floor. In addition, due to an efficient weathering of the micaschist bedrock, the original glacial surface of the few outcrops standing in the cirque floor is often not

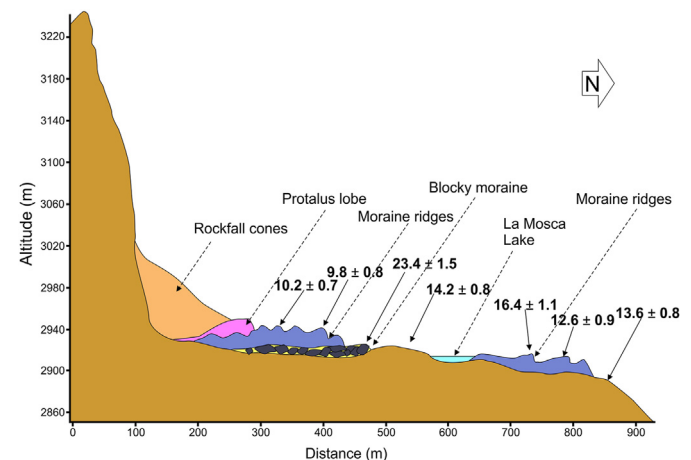


Fig. 3. Geomorphological transect along the Mulhacén cirque (S–N direction) showing the ^{10}Be CRE ages (in ka).

Table 2

Analytical data and cosmic ray exposure (CRE) ages. $^{10}\text{Be}/^9\text{Be}$ ratios were measured at the ASTER AMS facility. The numbers in italics correspond to the internal (analytical) uncertainty at 1σ level.

Sample name	Quartz weight (g)	Mass of carrier (^9Be mg)	ASTER cathode ID	$^{10}\text{Be}/^9\text{Be}$ (10^{-13}) corrected of chemical blank	Blank correction (%)	$[^{10}\text{Be}]$ (10^4 atoms g^{-1})	Age (ka)
MOSCA-2	39.7779	155.9	ICYQ	4.7124 ± 0.1461	0.52	37.321 ± 1.163	13.55 ± 0.8 (0.4)
MOSCA-3	29.2882	155.5	ICYR	3.6722 ± 0.1148	0.67	39.418 ± 1.238	14.20 ± 0.8 (0.4)
MOSCA-4	8.4979	158.3	ICYS	0.7182 ± 0.0350	3.31	27.047 ± 1.321	9.78 ± 0.8 (0.5)
MOSCA-5	5.9343	156.3	ICYT	1.2924 ± 0.0571	1.87	68.786 ± 3.045	23.41 ± 1.5 (0.9)
MOSCA-6	40.4572	153.2	ICYU	4.5547 ± 0.2008	0.54	34.864 ± 1.541	12.63 ± 0.9 (0.5)
MOSCA-7	21.5507	155.5	ICYV	3.1261 ± 0.1501	0.78	45.598 ± 2.194	16.42 ± 1.1 (0.7)
MOSCA-8	40.1676	156.3	ICYW	3.5672 ± 0.1130	0.68	28.061 ± 0.893	10.23 ± 0.7 (0.4)
^{10}Be Blank	—	—	—	—	—	—	—
MOSCA-BK	—	157.8	ICYP	—	—	—	—

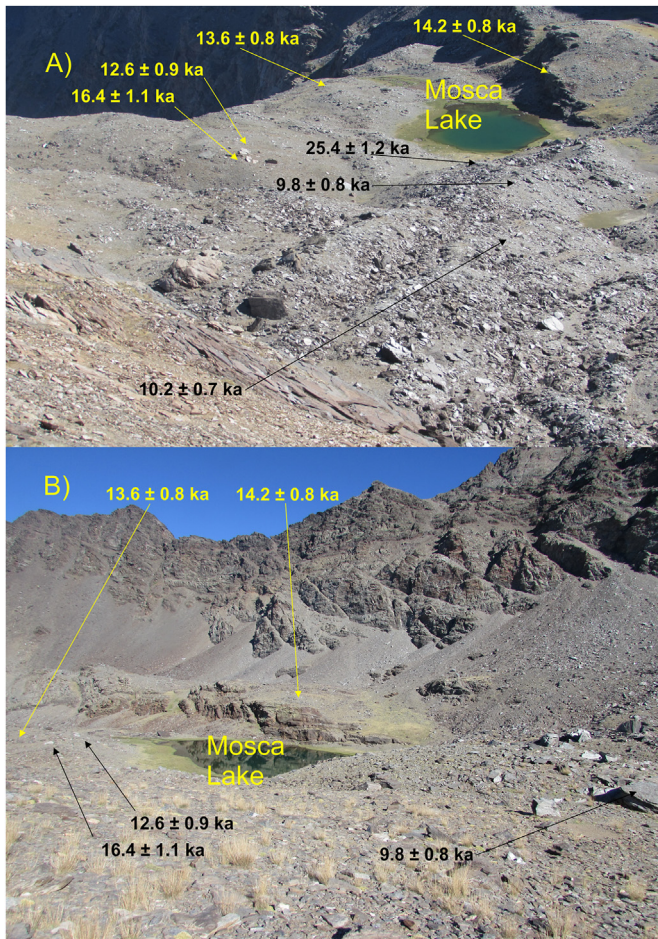


Fig. 4. Photos of the Mulhacén cirque floor, with the location of the CRE sampling sites and ^{10}Be ages. Panels A) and B) are oblique views of La Mosca Lake taken from the SE and E, respectively.

preserved and, therefore, only two polished surfaces were considered suitable for CRE dating. One sample was taken from a bedrock step below La Mosca Lake (MOSCA-2) and another one from a bedrock step above it (MOSCA-3) (Figs. 4 and 5).

The Mulhacén cirque ends downvalley in a large step that descends vertically from 2920 to 2600 m to the Valdecasillas gorge. The sample MOSCA-2 is located just on the edge of this step, next to two moraine ridges damming the La Mosca Lake. Due to the highly weathered surface of the rocks, only three boulders from these ridges appeared suitable for CRE dating (not affected by denudation, and standing out above the cirque floor): one from the outermost moraine (MOSCA-1) and two from the ridge closest to the lake (MOSCA-6 and MOSCA-7). The quartz content in sample MOSCA-1 was too low for ^{10}Be extraction and was considered non-suitable for further analyses.

A bedrock step above the lake was sampled (MOSCA-3). Large boulders within fine-grained matrix are distributed on this step. In contrast to the majority of moraines in the Sierra Nevada, composed of abundant fine sediments due to the weathering of the micaschists (Gómez-Ortiz et al., 2012; Palacios et al., 2016), this ridge preserved metric-size boulders. However, most of them were intensely fractured by frost shattering after their deposition, and only one sample from this landform was collected (MOSCA-5).

Overlapping this ridge, there is a moraine including both boulders and fine sediments. One boulder from this ridge was sampled, whose surface showed glacial striations ensuring that it has not

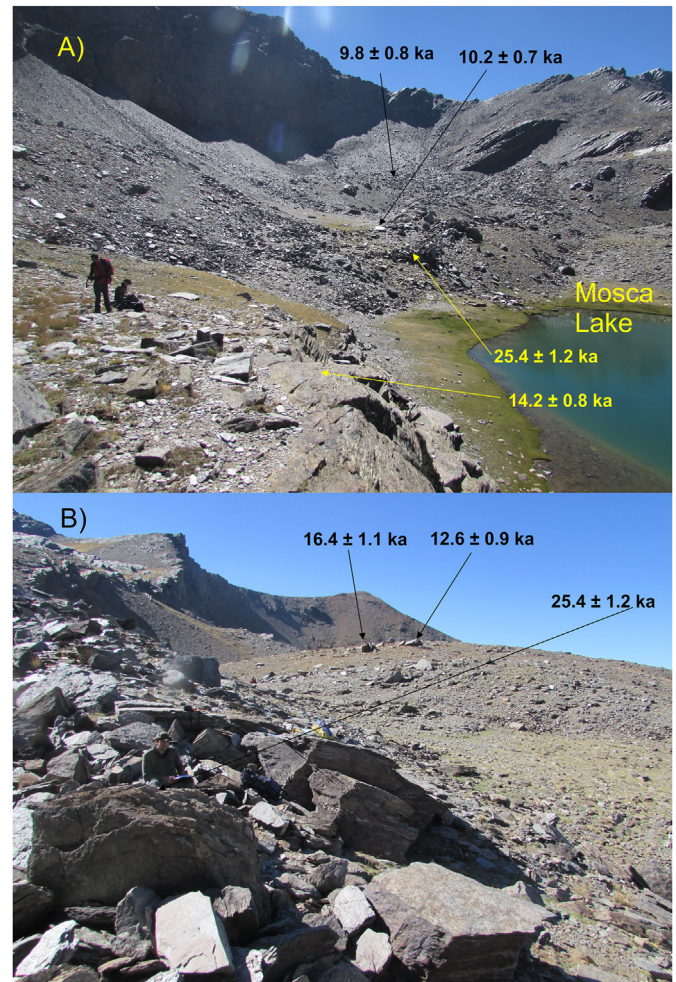


Fig. 5. Photos of the Mulhacén cirque floor, location of the CRE sampling sites and ^{10}Be CRE ages. A) Oblique view of La Mosca Lake from the W. B) Blocky moraine where the sample MOSCA-5 (with nuclide inheritance) was collected.

undergone major degradation since its deposition (MOSCA-4).

Above this ridge, there is a large area with a massive accumulation of boulders that corresponds to a large moraine system composed of several ridges. Due to the steep slope, the shape of some of these ridges has been altered by rock falls and slope readjustment, though they still show an arcuate morphology. All these moraines seem to be affected by slow flow of the surface sediments towards the base of the cirque, likely due to the presence of buried ice and permafrost patches such as those detected and monitored in the neighbouring Veleta cirque (Gómez-Ortiz et al., 2015, 2019). There are several depressions of collapse and subsidence features (Fig. 2) related to the degradation of the frozen mass located below the debris cover, which also affected the stability of the boulders. In addition, there are also abundant rocks fallen from the steep north wall of the Mulhacén, located only at less than 300 m from these deposits. Consequently, it was difficult to find boulders suitable for CRE dating and indicative of the age of stabilization of this moraine system. In fact, only one likely appropriate boulder in an external ridge was sampled (MOSCA-8).

According to historical sources (Gómez-Ortiz et al., 2009, 2015, 2018), the LIA glacier did not reach these outermost moraines and only occupied the innermost moraine systems closer to the northern Mulhacén rock wall, which is very active supplying debris to the talus cones. Currently, an active protalus lobe at the foot of

the rock wall indicates the occurrence of permafrost conditions at this site.

4.2. CRE results

As usual, we highly recommend using only the internal (analytical) errors, when the ^{10}Be ages are compared amongst them (at the study site and at the other sites), because they are all equally impacted by the production rate uncertainty – the production rate uncertainty has to be considered when the ^{10}Be ages are compared to other chronological data.

The CRE results are presented in Table 2, and Figs. 6 and 7. The two samples from polished bedrock lead to indistinguishable CRE ages: 13.5 ± 0.8 ka (MOSCA-2) and 14.2 ± 0.8 (MOSCA-3). Assuming that the age of the bedrock samples reveals the age of the final ice retreat in the mouth of the cirque, this leads to a mean CRE age of 13.8 ± 0.8 ka ($n = 2$).

The two samples from the moraine just below La Mosca Lake yielded to CRE ages of 12.6 ± 0.9 ka (MOSCA-6) and 16.4 ± 1.1 ka (MOSCA-7). Therefore, although from the same moraine, one boulder leads to an age 1.6 ka younger than the age of the bedrock surface where it rests, whereas the other leads to an age 2.2 ka older, respectively. Considering that the exposure age of the sample MOSCA-7 is older than that of the bedrock where it rests, it can be considered an outlier.

The samples taken above the lake – one located in a moraine of one of the lower ridges (MOSCA-4, 9.8 ± 0.8 ka) and the other in a moraine of one of the highest ridges (MOSCA-8, 10.2 ± 0.7 ka) – lead to indistinguishable CRE ages whose mean value is 10.0 ± 0.7 ka ($n = 2$). The deposition of these boulders resulted from different glacial events separated by only a few hundred years. The sample taken from the ridge formed by large boulders, located above the

lake, leads to a CRE age of 23.4 ± 1.5 ka (MOSCA-5). Significantly older than the landforms located more distant from the cirque wall (mean CRE age of 14.1 ± 0.9 ka ($n = 4$)), this age is inconsistent with the geomorphological sequence, probably due to nuclide inheritance.

5. Discussion

The results obtained in this work provide an approximate chronology of glacial retreat in the Mulhacén cirque, located at the foot of the highest peak in the Iberian Peninsula. The scarce number of landforms suitable to be sampled for the application of CRE dating impeded providing an accurate sequence of glacial oscillations for the transition from the Late Glacial to the Early Holocene, when most of the cirque became ice-free. This is due to the very intense geomorphological processes of the northern wall of the Mulhacén, with intense rock fall activity generating large talus cones that have covered some of the most recent moraines. In addition, the micaschist bedrock fractures very easily and it is therefore very difficult to find original glacial surfaces in boulders or bedrock outcrops.

5.1. Sequence of geomorphological phases in the mulhacén cirque

Despite the small number of available samples to which the CRE dating method can be applied with confidence, the combination of the results obtained in this study with those from previous studies points to the occurrence of a number of geomorphological phases inside the Mulhacén cirque (Table 2, and Figs. 6 and 7):

- (i) The deglaciation of most of the cirque culminated approximately at 14 ka – including the area where La Mosca Lake is

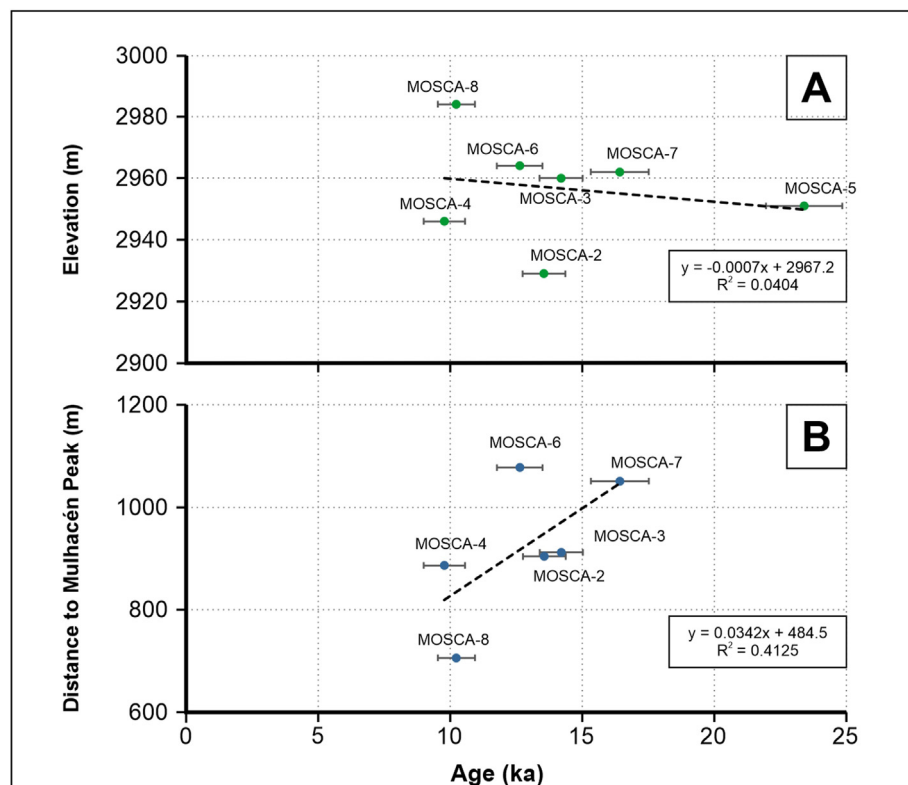


Fig. 6. CRE age correlation with: A) elevation, and B) distance to the Mulhacén headwall. In the panel B) we have removed the sample MOSCA-5 as being an outlier (cosmogenic nuclide inheritance). In the panel A) the correlation with altitude is very weak as all the samples are located on the flat floor of the cirque.

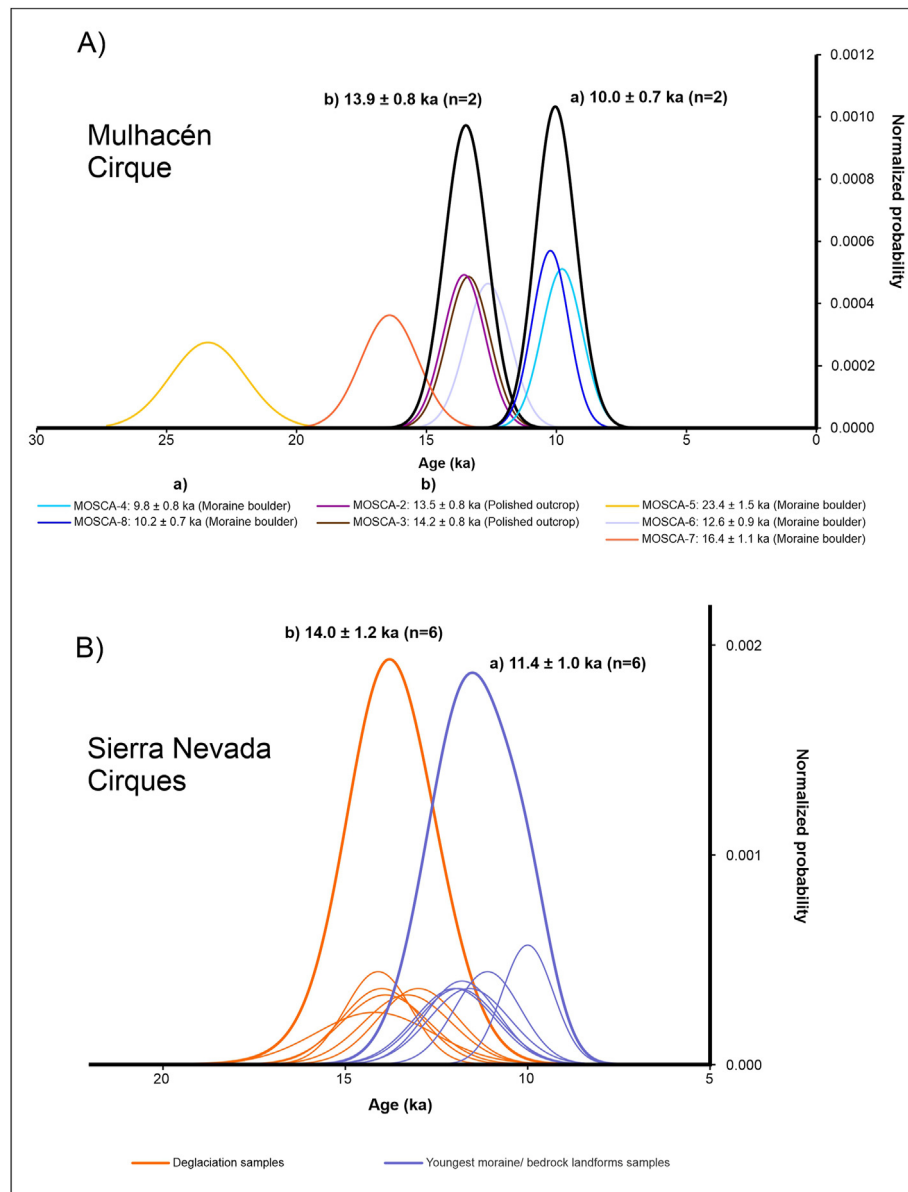


Fig. 7. Probability density plots of CRE ages for different chronostratigraphic units in the A) Mulhacén cirque (data shown in Table 3) and B) in the Sierra Nevada cirques (data shown in Table 4). Panels correspond to different stages according to the chronostratigraphy: a) Deglaciation of the Mulhacén cirque floor after the Younger Dryas. b) Deglaciation of the cirque mouth at the beginning of the Bølling-Allerød interstadial. We have included two outlier samples, probably with cosmogenic nuclide inheritance (MOSCA-5 and MOSCA-7). The number associated with each averaged CRE age refers to the number of CRE ages from each geomorphological unit considered. We assume that this average is indicative of the age for each geomorphological phase detected in each cirque.

located —, which is related to the Bølling-Allerød Interstadial (B-A; 14.6–12.9 ka; GI-1 Greenland ice cores; Rasmussen et al., 2014). These results are compatible with the previous study that suggested that lake sedimentation started before 8.4 cal ka BP (Manzano et al., 2019).

- (ii) Other published works focusing on La Mosca Lake sediments reported glacial oscillations during the Late Holocene. Three coarse-grained layers deposited in the lake bottom were interpreted as indicating the existence of a glacier in the catchment at 2.8–2.7, 1.4–1.2 and 0.51–0.24 ka cal BP (Oliva and Gómez-Ortiz, 2012). The presence of a glacier during the LIA in this cirque was also confirmed by historical sources (Gómez-Ortiz et al., 2009, 2015, 2018). Our results show that the extent of these palaeoglaciers was spatially limited, with small features only located at the base of the wall in the

concavities that are currently occupied by talus cones. According to our results, the last Early Holocene glacial advance that generated moraines reached a distance of only 300 m from the foot of the wall.

- (iii) The set of moraines located between the talus cones and the lake, with up to 6 different ridges in less than 400 m, is indicative of repeated glacier advances and retreats in the early stages of the Holocene, towards ca. 10 ka. These Early Holocene glaciers had a significant debris cover provided by the northern rock wall of the Mulhacén cirque. Indeed, the abundance of boulders across this moraine system shows evidence of the very high debris supply on palaeoglaciers from the rock wall. During their retreat, the ice gradually melted leaving multiple collapse depressions.

The age difference between the samples that mark the deglaciation of the mouth of the cirque during the B-A Interstadial, and those of the moraines deposited at the bottom of the cirque during the Holocene, was also shown in a previous work (Oliva et al., 2015) by the application of Schmidt Hammer Exposure Dating, with higher rebound (R values) indicative of less weathered surfaces and thus younger ages. The moraine that led to a ^{10}Be CRE age of 14 ka coincided with an R value of 55 ± 4 , whereas the R values in the 10 ka ridge were higher, 64 ± 6 (Oliva et al., 2015).

- (iv) There are some samples that show evidence of cosmogenic nuclide inheritance. In fact, the outlier sample MOSCA-5 is related to the unique moraine formed by large boulders with no fine-grained sediments. The overestimated exposure age may be related to boulders fallen from the wall and transported supraglacially on the ice surface with no or very little surface readjustment. This process has earlier been inferred in other mountain cirques, especially in small ones with limited distance between the headwall and the moraines (Li et al., 2016; Çiner et al., 2017; Köse et al., 2019).
- (v) According to our results, there is no evidence of glacial activity during the Holocene Thermal Maximum (HTM: 9–5 ka, Renssen et al., 2009) in this cirque.
- (vi) The current intense geomorphological activity of the rock wall is shown by the formation of large rock fall cones and talus since the disappearance of the LIA glacier. These rock fall cones are underlain by permafrost, as it is demonstrated by the recent development of a protalus lobe at the foot of such rock wall (Serrano et al., 2018).

5.2. Common and diverse geomorphological phases in the Sierra Nevada cirques and their palaeoclimatic and topographic significance

In the Sierra Nevada, there is remnant evidence of two Late Pleistocene glacial cycles that are preserved in the form of moraine complexes in the southern valleys of the massif. During the last glacial cycle, the maximum ice extent slightly predated the LGM, as it has been shown by CRE dating of boulders from lateral moraines from the largest glacial valleys (Gómez-Ortiz et al., 2012, 2015; Palacios et al., 2016, 2019; Oliva et al., 2019). Moreover, the sequence of glacial phases inferred from several other cirques in the Sierra Nevada (Gómez-Ortiz et al., 2012, 2015; Palacios et al., 2016, 2019; Oliva et al., 2019) show a similar sequence of the last deglaciation to the one presented here from the Mulhacén cirque, whose main phases have been summarized in Table 3. It is important to consider that glacial cirques do not always form at the head of the valleys, such as in the Sierra Nevada where many develop on lateral slopes of the main valley more favourable for snow accumulation, especially on E- or NE-facing slopes.

Several common spatio-temporal patterns can be inferred with regards to the deglaciation (Figs. 7 and 8A) evolution in cirques of the Sierra Nevada (Table 3 and Fig. 7):

- (i) All the cirques studied in the Sierra Nevada were deglaciated at the beginning of the B-A, although glaciers either remained as small features or regenerated during the following cold phases. Six of the eight cirques studied Sierra Nevada show indistinguishable deglaciation ages based on samples obtained from polished bedrock surfaces, with an average of 14.0 ± 1.2 ka ($n = 6$) (samples from Palacios et al., 2016 and present work). Therefore, these datasets suggest that shortly after the onset of the B-A the valley floors were

ice-free and glaciers were confined within the cirques as small features at the foot of the highest rock walls and probably disappeared from many others (Fig. 8B and C).

- (ii) There are only two cirques (Río Seco and Caldereta) including samples of polished bedrock surfaces that suggest a more recent deglaciation (12.0 ± 1.1 ka, $n = 3$) (Palacios et al., 2016). They do not preserve evidence of later moraine formations or the development of large rock glaciers. These younger ages would reveal the presence of glaciers after the main deglaciation at the bottom of the cirque, as in other cirques, but they did not generate moraines or rock glaciers when the ice melted, most likely due to the low debris supply from relatively stable rock walls.
- (iii) In most cases, after the most important deglaciation phase following the LLGM, glaciers persisted in the cirques, or they regenerated during the YD (Fig. 8D). Some inner moraines in the cirques have a stabilization age similar (considering their uncertainties) to polished bedrock surfaces, with an average age of 11.4 ± 1.0 ka ($n = 6$) (Palacios et al., 2016 and present work).
- (iv) The importance of topographical constraints controlling the geomorphological evolution in each cirque of the Sierra Nevada after its final deglaciation at the end of the YD. Moreover, the topographical conditions of each cirque favoured the generation of different type of landforms:
 - a) The cirques with summit altitudes >3300 m and floors >2950 m, north exposed and with cirque walls >300 m high were the most climatically sensitive considering the geomorphological setting. They include evidence of glacier changes from the YD to the present. This is the case of the Veleta and Mulhacén cirques. But it is noteworthy that each one evolved differently: in the case of the Veleta cirque, a large polygenic moraine was formed (Gómez-Ortiz et al., 2009, 2012, 2015; Palacios et al., 2019) (Fig. 8E.4), whereas in the Mulhacén cirque a sequence of moraine ridges developed (Fig. 8E.5). During the HTM glaciers probably melted away in these cirques, but regenerated under the cold Neoglacial conditions prevailing during the Late Holocene, namely during the LIA (Gómez-Ortiz et al., 2009, 2012, 2015, 2018; Oliva and Gómez-Ortiz, 2012; Palacios et al., 2016). These Neoglacial advances enlarged the polygenic moraine in the Veleta cirque, and must have generated new moraine ridges in the Mulhacén cirque. However, the very intense geomorphological processes of the Mulhacén wall accumulating large masses of debris at the foot of the steep slope of the cirque and the readjustment of the moraine boulders have hidden the associated evidence.
 - b) Cirques with summit altitudes between 3000 and 3200 m, floors located above 2800 m, with small headwalls (elevation range <200 m) and east-facing produced only small proto-rock glaciers. This is the case of the Peñón Colorado, Río Seco and Caldereta cirques. In these cirques, where proto-rock glaciers developed, their fronts stabilized shortly after they formed (Fig. 8E.1).
 - c) In cirques with summit altitudes <3000 m and floors below 2800 m, the retreating glaciers left one or more moraines – or even none – depending on the intensity of the paraglacial readjustment of their walls rather than the climate oscillations, and no rock glaciers formed. This is the case of the Hoya de la Mora, Mojón de Trigo and Moro cirques (Fig. 8. E.3). These moraines are located between 400 and 700 m away from the cirque walls, showing evidence of the small size of the YD glaciers.

Table 3

Location, main topographic characteristics, geomorphological units, and average CRE ages from the cirques studied in the Sierra Nevada compared to the Mulhacén cirque.

Cirque/valley	Location ^a	Cirque elevation range ^b (m a.s.l.) and (m)	Length ^c (m)	Aspect ^d	Deglaciation (ka) ^e	Youngest moraine/ bedrock (ka) ^f	Distance from headwall to the youngest moraine (m) ⁷	Rock glacier and protalus lobe landforms (ka) ^g	Neoglacial landforms (ka/ CE) ^h	References
La Mora/San Juan	37°5'43"N 3°22'57"W	2609–2350 (259)	600	NE	13.9 ± 1.2 (n = 2)	4 moraine ridges	400	—		Palacios et al. (2016)
Mojón del Trigo/San Juan	37°5'22"N 3°22'36"W	2609–2350 (259)	800	E	14.5 ± 1.2 (n = 2)	3 moraine ridges	600	—		Palacios et al. (2016)
El Moro/San Juan	37°4'28"N 3°22'22"W	2925–2790 (135)	700	E	14.0 ± 1.1 (n = 2)	1 ridge	500			Palacios et al. (2016)
Cartujo/Dílar	37°3'9"N 3°22'57"W	3152–2700 (452)	1400	N	14.2 ± 1.6 (n = 2)	No data		Rock glacier From 11.4 ± 1.0 to 6.4 ± 0.6		Palacios et al. (2016)
Peñón Colorado/Lanjarón	37°1'56"N 3°24'23"W	3113–2950 (163)	600	E	13.0 ± 1.1 (n = 4)	3 ridges No data		Proto-rock glacier 10.5 ± 0.9		Palacios et al. (2016)
Río Seco/Río Seco	37°2'55"N 3°20'39"W	3141–3000 (141)	600	E		Bedrock 11.9 ± 1.1 (n = 1)		Proto-rock glacier 9.0 ± 0.8		Palacios et al. (2016)
Caldereta/Mulhacén	37°3'5"N 3°19'32"W	3182–3000 (182)	900	E		Bedrock 12.0 ± 1.1 (n = 2)		Rock glacier from 13.1 ± 1.2 to 6.3 ± 0.5		Palacios et al. (2016)
Corral del Veleta/Guarmón	37°3'35"N 3°21'57"W	3396–3000 (396)	500	N	No data	Large polygenic ridge		Rock glacier from 1950 CE	Polygenic LIA ridge From 1355 to 1900 CE	Palacios et al. (2019)
Mulhacén cirque	37° 3'36"N 3°18'57"W	3479–2900 (579)	950	N	14.1 ± 0.9 (n = 1) (a)	6 ridges 10.0 ± 0.7 (n = 2)(a)	700	Protalus lobe from 1900 CE (b)		(a) Present work (b) Serrano et al. (2018)

^a Geographic coordinates of the center point of the cirque floor.^b Maximum and minimum elevation of the cirque and elevation range.^c Cirque length. From the summit to the lower sector measured on the map. It is necessary to consider that many cirques are wider than they are long.^d Aspect. It is necessary to consider that many cirques do not coincide with the head of the valley where they are located, but rather they are housed on one of its slopes with a more appropriate orientation for the accumulation of snow.^e Deglaciation age of the cirque according to the CRE ages obtained from bedrock outcrops on its bottom.^f Number of moraines and their CRE age in ka or CE located into the cirque. When no moraine ages are available, the age corresponds to dated bedrock surfaces.^g Rock glaciers and protalus lobe located in the cirque and the stabilization CRE age of its front and its root, when available.^h Neoglacial landforms present in the cirque.

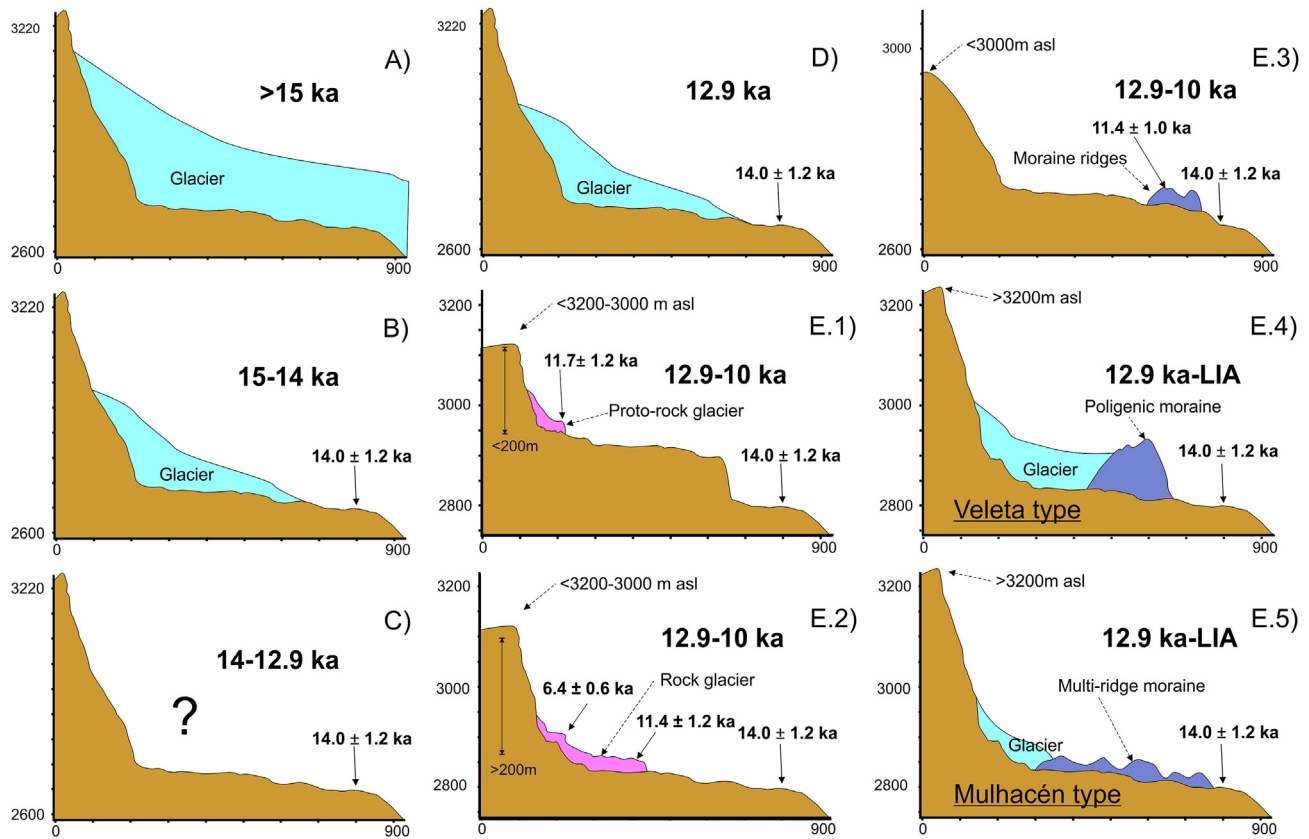


Fig. 8. Synthetic evolution model of the deglaciation phases in the cirques of the Sierra Nevada. A) The glaciers filled the cirques during the OD, until just before the onset of the B-A Interstadial. B) The mouth of most of the cirques was deglaciated during the B-A Interstadial. C) Glaciers might have disappeared from the Sierra Nevada cirques. D) Most of the cirques hosted new small glaciers during the YD. After this phase, the cirques evolved differently, according to their topographic characteristics. E.1) Cirques with summits at 3000–3200 m and floors at >2800 m, with small headwalls (<200 m of altitude range) and east-facing produced only small proto-rock glaciers. E.2) Cirques with summits at 3000–3200 m and floors at >2800 m, with steep and long headwalls (>300 m of altitude range) developed larger rock glacier complexes, especially if they are north facing. E.3) Cirques with summits at <3000 m and floors at <2800 m. The shrinking glaciers left one or more moraines – or even none – depending on the intensity of the paraglacial readjustment of their surrounding walls. Cirques with summits at >3300 m and floors at >2950 m, north-facing and with >300-m-high walls recorded geomorphic evidence from glacier changes from the YD to present. This is the case of the Veleta and Mulhacén cirques, but their evolution was different. E.4) Veleta palaeoglacier formed only a large polygenic moraine. E.5) Mulhacén palaeoglacier developed a sequence of moraine ridges.

- (v) Except in the case of the Veleta and Mulhacén cirques, the landscape of the rest of the cirques is similar to that existing during the HTM. No new glacial landforms have formed since and they have been affected only by limited periglacial and slope processes during Late Holocene cold phases (Oliva, 2009; Oliva and Gómez-Ortiz, 2012; Oliva et al., 2010, 2011 and 2020).
- (vi) Based on the evolution and chronology of the Sierra Nevada glacial cirques, we assume that the origin of the rock glaciers they host are related to the process of deglaciation that occurred at the beginning of warm periods in connection with paraglacial processes which triggered an intense geomorphological activity of the rock walls (Kleman and Stroeven, 1997; Ballantyne, 2002, 2013; Knight et al., 2018; Serrano et al., 2018).
- (vii) As in other cirques of the Sierra Nevada at the end of the Late Pleistocene glacial phases, the end of Neoglaciation with the disappearance of the LIA glaciers has favoured the development of a small rock glacier in the Veleta cirque (Gómez-Ortiz et al., 2015, 2019) and a protalus lobe in the Mulhacén cirque (Serrano et al., 2018), where small isolated permafrost patches exist under the debris cover (Oliva et al., 2018; Serrano et al., 2018). These landforms are geoindicators of the end of cold periods and are out of balance with current

climate conditions, and therefore, tend to become inactive (Oliva et al., 2018; Gómez-Ortiz et al., 2019).

5.3. The typology of the cirques in Sierra Nevada in the context of the Iberian Peninsula

Studies similar to those conducted in the Sierra Nevada have been carried out in other Iberian mountain ranges, although most of them focused on individual cirques, with the exception of some studies in the Pyrenees. The chronology of formation of different landforms in the cirques of the Sierra Nevada is highly (Table 4 and Fig. 9A) similar to the periods of formation of analogous geomorphological features in other Iberian cirques (Table 4).

- (i) Based on the available literature, we have analysed a total of 26 Iberian cirques, where the maximum and minimum CRE ages of deglaciation at their mouth vary from 16.3 ± 3.3 ka to 13.2 ± 0.7 ka, considering either the time of stabilization of external moraines, or the outcropping of the bedrock due to the disappearance of the ice (Table 4). The average age of deglaciation taking into account all these cirques is 15.1 ± 1.3 ka ($n = 21$). According to marine and terrestrial records from the Iberian Peninsula and surrounding areas (Fletcher et al., 2010a, 2010b; Moreno et al., 2014; López-Sáez et al., 2020),

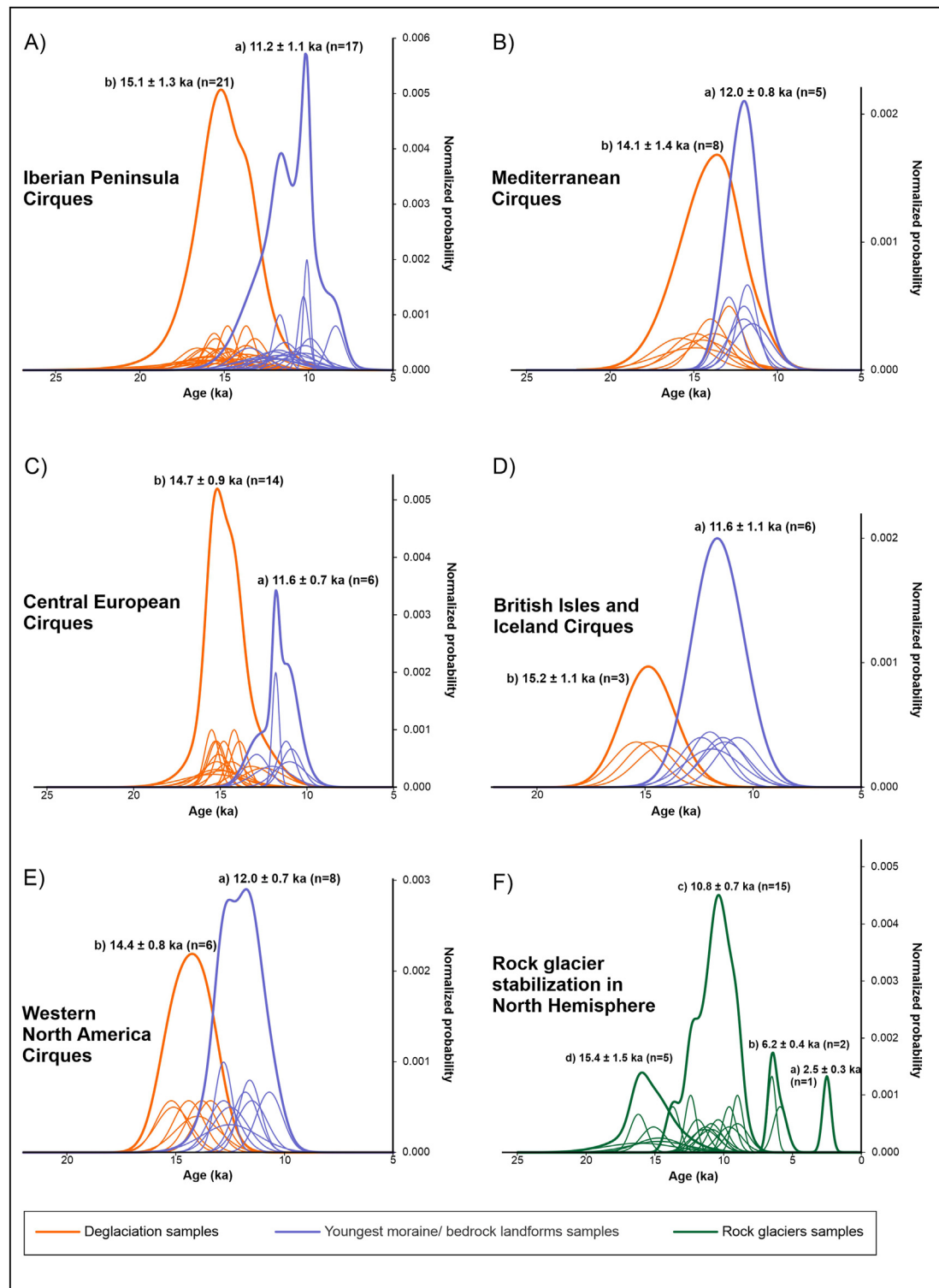


Fig. 9. Probability density plots of CRE ages for different chronostratigraphical units in A) The Iberian Peninsula cirques (data shown in Table 4); B) The Mediterranean cirques (outside Iberian Peninsula) (data shown in Table 5); C) The Central European cirques (data shown in Table 6); D) The British Isles and Iceland cirques; E) The Western North America cirques (data shown in Table 8); F) Rock glacier front stabilization in the cirques analysed in the North Hemisphere (data shown in Tables 3–8). For Fig. 9B) and C), D) and E) the plots are clustered in a) Deglaciation of the cirque floor after the YD (ages of the stabilization of the youngest moraine and polished bedrock surfaces); b) Deglaciation of the mouth of the cirque, at the beginning of the B-A Interstadial (ages of the stabilization of the oldest moraine inside the cirque and polished bedrock surfaces). For the Panel F) the plots are clustered in a) Rock glacier front stabilization after Neoglaciation advances; b) Rock glacier front stabilization after the Younger Dryas; c) Rock glacier front stabilization after at the beginning of the B-A Interstadial. The number associated with each averaged CRE age refers to the number of CRE ages from each geomorphological unit considered.

Table 4
Location, main topographic characteristics, geomorphological units, and average CRE ages of the cirques studied in the rest of Iberian Peninsula (outside Sierra Nevada). All CRE ages are updated following [Oliva et al. \(2019\)](#).

Cirque/Valley and rock type	Massif/range ^a	Elevation (m a.s.l.) and geographic coordinates ^b	Aspect ^c	Deglaciation of the cirque (ka) ^d	Youngest: moraine/bedrock landforms (ka) ^e	Distance from headwall to the youngest moraine (m)	Rock glacier/debris-covered glacier/other landforms (ka) ^f	Neoglacial landforms (ka) ^g	References
Cinco Lagunas/Pinar (Granite)	Sierra de Gredos/Central Range	2572 40°15'22"N 5°18'24"W	NNE	16.3 ± 3.3 (n = 2)	Bedrock 10.3 ± 1.3 (n = 3)		Protalus rampart,	—	Palacios et al. (2011)
Gredos (Granite)	Sierra de Gredos/Central Range	2591 40°14'56"N 5°17'58"W	N	15.9 ± 1.0 (n = 2)				—	Palacios et al. (2012a)
Cuerpo de Hombre (Granite)	Sierra de Gredos/Central Range	2399 40°17'32"N 5°45'14"W	NW	15.1 ± 1.0 (n = 3)	Moraine 12.1 ± 1.2 (n = 1)	600	Rock avalanche	—	Carrasco et al. (2015)
Peñalara/Lozoya (Gneis)	Sierra de Guadarrama/Central Range	2428 40°50'60"N 3°58'1" W	ESE	15.9 ± 1.0 (n = 2)	Bedrock 11.7 ± 0.4 (n = 1)		Proto-rock glacier 16.1 ± 2.5 (n = 1)	—	Palacios et al. (2012b)
Hoyo Grande/Lozoya (Gneis)	Sierra de Guadarrama/Central Range	2209 40°58'46"N 3°50'51"W	SE	15.6 ± 0.6 (n = 2)					Carrasco et al. (2016)
San Lorenzo/Najerilla (Conglomerates)	Sierra de la Demanda/Iberian Range	2271 42°14'33" N 2°58'22" W	SE	16.1 ± 1.0 (n = 2)			Debris-covered glacier 9.0 ± 0.4 (n = 3)	—	Fernández-Fernández et al. (2017)
Mencilla/Arlanzón (Conglomerates)	Sierra de la Demanda/Iberian Range	1932 42°11'9"N 3°18'44"W	NNE				Debris-covered glacier 6.5 ± 0.3 (n = 8)	—	Fernández-Fernández et al. (2017)
Peña Negra/Mayor (Conglomerates)	Sierra de la Cebollera/Iberian Range	2023 m 42°2'39" 2°45'35"W	ENE	16.6 ± 1.0 (n = 2)	Bedrock 13.5 ± 1.0 (n = 1)		Rock glacier 15.1 ± 0.9 (n = 3)	—	García-Ruiz et al. (2020a)
Monasterio (Quartzites)	Montaña Central/Cantabrian Mountains	2019 43°5'1"N 5°20'24"W	N	14.8 ± 0.5 (n = 5)			Rock glacier 13.7 ± 0.5 (n = 5)	—	Rodríguez-Rodríguez et al. (2017)
Silván (Quartzites)	Montaña Central/Cantabrian Mountains	1935 43°2'31"N 5°21'14"W	ENE				Rock glacier 16.2 ± 0.6 (n = 5)	—	Rodríguez-Rodríguez et al. (2016)
Malniu-Guils cirques (Granite)	Cerdanya/Eastern Pyrenees	2692 42°29'8"N 1°47'31"E	S	14.8 ± 2.0 (n = 1)			Rock glacier 14.7 ± 1.6 (n = 1)	—	Andrés et al. (2019)
Perafita/Arànsér (Granite)	Cerdanya/Eastern Pyrenees	2761 42°26'59"N 1°34'53"E	E	13.7 ± 0.5 (n = 1)	Moraine 12.6 ± 1.7 (n = 1)		Rock glacier From 14.7 ± 2.1 to 8.6 ± 1.1	—	Andrés et al. (2019)
Bassières/Escale (Granite)	Eastern Pyrenees	2763 42°37'0"N 1°57'34"E	N	15.8 ± 1.7 (n = 2)	Moraine 11.7 ± 1.5 (n = 2)	1200		—	Crest et al. (2017); Tomkins et al. (2018)
Rec de la Grava/ (Granite)	Cerdanya/Eastern Pyrenees	2763 42°37'7"N 1°57'16"E	S		Bedrock 11.5 ± 2.0 (n = 3)	1100		—	Crest et al. (2017); Tomkins et al. (2018)
Picot Ariège valley (Granite)	Eastern Pyrenees	2797 42°40'34"N 1°28'55"E	NW	15.5 ± 0.7 (n = 4)	Bedrock 8.4 ± 0.5 (n = 1)		Rock glacier From 7.2 ± 0.4 to 1.4 ± 0.2	—	Jomelli et al. (2020)
Médécourbe/Ariège valley (Granite)	Eastern Pyrenees	2914 42°36'13"N 1°26'31"E	N	13.2 ± 0.7 (n = 2)	Bedrock/moraine 9.9 ± 0.7 (n = 3)			—	Jomelli et al. (2020)
Mulleres*/Noguera Ribagorçana (Granite)	Central Pyrenees	3010 42°37'44"N 0°41'54"E	E	13.7 ± 0.9 (n = 3)	Moraine 10.3 ± 0.3 (n = 2)			—	Pallàs et al. (2006)
	Central Pyrenees		W	16.3 ± 2.2 (n = 1)	Moraine 10.1 ± 0.2 (n = 2)		Rock glacier (active)		Pallàs et al. (2006)

(continued on next page)

Table 4 (continued)

Cirque/Valley and rock type	Massif/range ^a	Elevation (m a.s.l.) and geographic coordinates ^b	Aspect ^c	Deglaciation of the cirque (ka) ^d	Youngest: moraine/bedrock landforms (ka) ^e	Distance from headwall to the youngest moraine (m)	Rock glacier/debris-covered glacier/other landforms (ka) ^f	Neoglacial landforms (ka) ^g	References
Bessiberri* /Noguera Ribagorçana (Granite)		3017 42°35'41"N 0°49'13"E							
Maladeta/Esera (Granite)	Central Pyrenees	3323 42°38'47"N 0°38'25"E	N	13.7 ± 1.4 (n = 2)	Bedrock/moraine 11.8 ± 1.1 (n = 2)	1200		From 4.5 to 1.1 moraine	Crest et al. (2017); Tomkins et al. (2018)
Marboré/Pineta (Sandstones)	Central Pyrenees	3348 42°40'32"N 0°2'4"E	N					5.6 ± 0.6 3.6 ± 0.4 1.1 ± 0.1 and 1.1 moraines	García-Ruiz et al. (2014)
Arrémoulit/Osseau (Granite)	Central Pyrenees	2821 42°50'5"N 0°19'51"W	N		Bedrock 10.2 ± 0.9 (n = 2)			—	Palacios et al. (2017a)
Balaitus/Agua Limpia (Granite)	Central Pyrenees	3147 42°50'20"N 0°17'25"W	S	14.6 ± 2.0	Bedrock 11.0 ± 1.4 (n = 2)			LIA moraine	Palacios et al. (2017a)
Bachimaña/Caldarés (Granite)	Central Pyrenees	2728 42°47'54"N 0°13'2"W	S	12.9 ± 1.5 (n = 3)				—	Palacios et al. (2017a)
Brazato/Caldarés (Granite)	Central Pyrenees	2722 42°44'21"N 0°12'33"W	NNW	14.5 ± 1.2	Bedrock 11.4 ± 0.8		Rock glacier 6.1 ± 0.3 (n = 2)	—	Palacios et al. (2017a)
Catieras/Caldarés (Granite)	Central Pyrenees	2564 42°43'4"N 0°11'18"W	W	15.9 ± 1.6	Moraine 10.9 ± 1.2	600	Rock glacier 12.0 ± 1.3 (n = 3)	—	Palacios et al. (2017a)
Piniecho/Caldarés (Granite)	Central Pyrenees	2696 42°43'43"N 0°12'12"W	W	15.6 ± 2.3 (n = 4)	Moraine 12.4 ± 1.9	500	Rock glacier 13.0 ± 1.3 (n = 4)	—	Palacios et al. (2017a)

^a Name of the cirque within the mountain range.^b Elevation and geographic coordinates of the highest summit of the cirque.^c Main aspect of the cirque.^d CRE age showing the deglaciation of the cirque. Note that small glaciers may have remained at the foot of the cirque walls. All ages are related to the bedrock and/or moraines distributed at the mouth of the cirque.^e CRE ages indicating the final deglaciation of the cirque. All ages correspond to bedrock or moraines located in the highest parts of the cirque.^f CRE ages reporting the stabilization of the rock glacier fronts. If there are two ages, the second one corresponds to the stabilization of the roots of the rock glacier. Other debris landforms (debris-covered glacier, proglacial rampart, rock avalanches, etc.) located in the cirque floor are also included, with their age of stabilization.^g Existence of landforms generated by Neoglacial advances with the available CRE ages, if existing.

Table 5

Location, main topographic characteristics, geomorphological units, and average CRE ages of the cirques studied in the Mediterranean region (Iberian Peninsula not included). All CRE ages are updated.

Cirque/Valley	Massif/range ^a	Elevation (m a.s.l.) and coordinates ^b	Aspect ^c	Deglaciation of the cirque (ka) ^d	Youngest moraine (ka) ^e	Distance from headwall to the youngest moraine (m)	Rock glacier landforms (ka) ^f	Neoglacial landforms (ka) ^g	References
Kisbe/Sayacak	Mt. Dedegol Mts Taurus Anatolia Pen.	2750 37°40'40"N 31°15'16"E	N		11.5 ± 1.1 (n = 2)	2500			Köse et al. (2019)
Karagol	Mt. Dedegol Mts Taurus Anatolia Pen.	2900 37°38'35"N 31°17'25"E	E	15.8 ± 1.6 (n = 1)	12.0 ± 1.0	1800			Köse et al. (2019)
North Çimi	Central Taurus Anatolia Pen.	2411 36°57'21"N 31°59'32"E	E	13.7 ± 0.8 (n = 1)	8.1 ± 0.9^h (n = 2)	1500			Sarıkaya et al. (2017), ^h
South Çimi	Central Taurus Anatolia Pen.	2411 36°57'28"N 31°58'55"E	E	14.9 ± 1.4 (n = 5)	7.3 ± 0.6^h (n = 4)	2500			Sarıkaya et al. (2017), ^h
Güneycik	Central Taurus Anatolia Pen.	2440 37°1'41"N 31°59'24"E	E	14.5 ± 1.7 (n = 4)				5.9 ± 0.5 (n = 4)	Sarıkaya et al. (2017)
Çündüre	Central Taurus Anatolia Pen.	2638 36°58'40"N 32°1'46"E	NE	14.9 ± 2.3 (n = 3)					Sarıkaya et al. (2017)
Megala Kazania	Mount Olympus Balkans	2918 40°05'0"N 22°21'0"E	NNE	13.8 ± 1.4 (n = 3)	12.0 ± 0.8 (n = 2)	800			Styllas et al. (2018)
Throne of Zeus	Mount Olympus Balkans	2918 40°05'30"N 22°21'30"E	NNW	14.0 ± 1.0 (n = 4)				2.5 ± 0.3 (n = 4) and LIA	Styllas et al. (2018)
Velez Mountain	Dinaric Mts.	1965 43°19'02"N 18°2'6"E	N	14.9 ± 1.1 (n = 2)					Žebre et al. (2019)
Irhzer n'Likemt	Akusal Atlas Mts. Morocco	3555 31°7'39"N 7°49'56"W	N		12.9 ± 0.7 (n = 2)	1200			Hughes et al. (2018)
Azib Mzik	Akusal Atlas Mts. Morocco	3129 31°6'53"N 7°56'28"W	NE		11.8 ± 0.6 (n = 3)	800			Hughes et al. (2018)

^a Name of the cirque within the mountain range.^b Elevation and geographic coordinates of the highest summit of the cirque.^c Main aspect of the cirque.^d CRE age showing the deglaciation of the cirque, though small glaciers may have remained at the foot of the cirque walls. All ages are related to the bedrock and/or moraines distributed at the mouth of the cirque.^e CRE ages indicating the final deglaciation of the cirque. All ages correspond to bedrock or moraines located in the highest parts of the cirque.^f CRE ages reporting the stabilization of the rock glacier fronts. If there are two ages, the second one corresponds to the stabilization of the roots of the rock glacier.^g Existence of landforms generated by Neoglacial advances with the available CRE ages, if existing.^h These moraines are not included in the statistical analysis of Fig. 11, as they are considered exceptional. Ages obtained in limestone under heavy erosion.

Table 6

Location, main topographic characteristics, geomorphological units, and CRE ages of the cirques studied in the Central European region (outside Sierra Nevada). All CRE ages are updated.

Cirque/Valley	Massif/range ^a	Elevation (m a.s.l.) and coordinates ^b	Aspect ^c	Deglaciation of the cirque (ka) ^d	Youngest moraine (ka) ^e	Distance from headwall to the youngest moraine (m)	Rock glacier landforms (ka) ^f	Neoglacial landforms (ka) ^g	References
North Mohoru	Parâng Mts. Romanian Carpathians	2365 45°20'27"N 23°36'25"E	N	13.2 ± 1.1 ka (n = 5)	11.8 ± 0.2 ka (n = 2)	500			Gheorghiu et al. (2015)
Zanoaga Mare	Parâng Mts. Romanian Carpathians	2278 45°21'4"N 23°31'60"E	N	13.7 ± 1.2 ka (n = 4)	11.0 ± 0.9 ka (n = 2)	800			Gheorghiu et al. (2015)
Galcescu	Parâng Mts. Romanian Carpathians	2519 45°20'24"N 23°32'25"E	N	15.2 ± 1.3 (n = 1)	12.0 ± 1.1 ka (n = 3)	800			Gheorghiu et al. (2015)
Spitze Rumer Spitze	Karwendel Mts. North Alps	2454 47°19'13"N 11°25'35"E	N				From 12.4 ± 0.4 to 9.6 ± 0.6 (n = 7)		Moran et al. (2016)
Mandlsplitze	Karwendel Mts. North Alps	2370 47°19'7"N 11°24'25"E	N				10.9 ± 0.8 (n = 4)		Moran et al. (2016)
Nefcerská	High Tatra Western Carpathians	2428 49°10'14"N 20°1'37"E	N	14.2 ± 0.4 (n = 2)			11.3 ± 0.9 (n = 3)		Zasadni et al. (2020)
Suchá vážecká	High Tatra Western Carpathians	2350 49°9'47"N 20°0'48"E	S	14.9 ± 1.4 (n = 2)			10.9 ± 1.0 (n = 3)		Zasadni et al. (2020)
Mlynická	High Tatra Western Carpathians	2428 49°10'14"N 20°1'37"E	N				10.4 ± 0.7 (n = 3)		Zasadni et al. (2020)
Hincova	High Tatra Western Carpathians	2438 49°11'11"N 20°3'38"E	SE	14.8 ± 0.5 (n = 1)			11.9 ± 0.7 (n = 3)		Zasadni et al. (2020)
Kasprowy Wierch	High Tatra Western Carpathians	1987 49°13'55"N 19°58'54"E	N	14.4 ± 0.9 ka (n = 4)					Makos et al. (2018)
Bystra Sucha Woda	High Tatra Western Carpathians	2235 49°13'6"N 20°1'45"E	N	15.5 ± 0.4 ka (n = 5)					Makos et al. (2018)
Biata Woda	High Tatra Western Carpathians	2300 49°13'10"N 20°0'34"E	N	15.2 ± 0.9 ka (n = 10)					Makos et al. (2018)
Piec Stawow Polskich valley	High Tatra Western Carpathians	2503 49°10'46"N 20°5'16"E	N	15.1 ± 0.7 ka (n = 5)	10.9 ± 0.6 ka (n = 5)	700			Makos et al. (2018)
Velká Studená	High Tatra Western Carpathians	2383 49°10'59"N 20°8'40"E	E	15.2 ± 0.5 (n = 4)					Engel et al. (2015)
Malá Studená	High Tatra Western Carpathians	2627 49°12'9"N 20°11'46"E	SE	13.9 ± 0.5 (n = 1)	11.2 ± 0.5 (n = 1)	500			Engel et al. (2015)
Sněžka Úpa valley	Krkonoše Mountains	1602 50°44'10"N 15°44'25"E	S	15.3 ± 0.5 (n = 1)					Engel et al. (2017)
Snowy cirque	Krkonoše Mountains	1509 50°46'39"N 15°34'03"E	NE	15.4 ± 1.8 (n = 1)	12.9 ± 0.7 (n = 1)	400			Engel et al. (2017)

^a Name of the cirque within the mountain range.

^b Elevation and geographic coordinates of the highest summit of the cirque.

^c Main aspect of the cirque.

^d CRE age showing the deglaciation of the cirque, though small glaciers may have remained at the foot of the cirque walls. All ages are related to the moraines distributed at the mouth of the cirque.

^e CRE ages indicating the final deglaciation of the cirque. All ages correspond to moraines located in the highest parts of the cirque.

^f CRE ages reporting the stabilization of the rock glacier fronts. If there are two ages, the second one corresponds to the stabilization of the roots of the rock glacier.

^g Existence of landforms generated by Neoglacial advances with the available CRE ages, if existing.

a sudden temperature increase that led to values similar to present is recorded at the beginning of B-A. The accelerated deglaciation of the cirques probably during the B-A has been detected in many other cirques in Iberian mountains (Palacios et al., 2017b), such as the Central Range (Palacios et al., 2011; Palacios et al., 2012a, 2012b; Carrasco et al., 2015), Iberian Range (Fernández-Fernández et al., 2017; García-Ruiz et al., 2020a), Central Cantabrian Mountains

(Rodríguez-Rodríguez et al., 2017) and the Pyrenees (Pallàs et al., 2006, 2010; Delmas, 2015; Palacios et al., 2017a; Crest et al., 2017; Tomkins et al., 2018; Andrés et al., 2019; Jomelli et al., 2020).

(ii) Although they still need to be studied in much more detail, YD glaciers existed within the cirques of other Iberian mountain ranges (García-Ruiz et al., 2016). There are few studies on YD related moraines in the in the Pyrenees (Pallàs

Table 7

Location, main topographic characteristics, geomorphological units, and average CRE ages of the cirques studied in the British Isles and Iceland. All CRE ages are updated.

Cirque/Valley	Massif/ Range ^a	Elevation (m a.s.l.) and coordinates ^b	Aspect ^c	Deglaciation of the cirque (ka) ^d	Youngest moraine/ bedrock (ka) ^e	Distance from headwall to the youngest moraine (m)	Rock glacier landforms (ka) ^f	Neoglacial landforms ^g	References
Corranabinn Lough	Mayo Western Ireland	670 53°57'40"N 9°41'15"W	NNE	15.4 ± 1.1 (n = 4)					Barth et al. (2018)
Glascairns Hill	Donegal NW Ireland	580 54°46'15"N 8° 1'42"W	NE	15.9 ± 1.1 (n = 8)	12.0 ± 0.9 (n = 4)	850			Barth et al. (2018)
Logaharry Lough	Mayo Western Ireland	620 53°37'38"N 9°42'10"W	NE	14.2 ± 1.2 (n = 4)					Barth et al. (2018)
Sruhauncullinmore	Mayo Western Ireland	803 53°38'29"N 9°47'31"W	NE		11.4 ± 1.0 (n = 4)	950	12.5 ± 1.1 (n = 5)		Barth et al. (2018)
Keskadale/ Newlands	Derwent Fells/Lake District British Isles	734 54°32'30"N 3°14'8"W	N		12.4 ± 1.0 ka (n = 2)	600			Hughes et al. (2019)
Ling Comb	Derwent Fells/Lake District British Isles	737 54°31'52"N 3°18'24"W	E		11.9 ± 1.3 ka (n = 4)	300			Hughes et al. (2019)
Fremri- Grjótárdalur West	Tröllaskagi Northern Iceland	1183 65°42'47"N 19°0'6.32"W	N		11.3 ± 1.1 (n = 2)	1500	10.8 ± 1.0 (n = 2)	Active rock glaciers	Fernández- Fernández et al. (2020)
Fremri- Grjótárdalur East	Tröllaskagi Northern Iceland	1183 65°42'47"N 19°0'6.32"W	N				9.4 ± 1.1 (n = 2)	Active rock glaciers	Fernández- Fernández et al. (2020)
Hólajökull	Tröllaskagi Northern Iceland	65°42'7"N 18°57'2"W	N		10.7 ± 1.0 (n = 2)	3000		Active debris covered glacier	Fernández- Fernández et al. (2020)

^a Name of the cirque within the mountain range.^b Elevation and geographic coordinates of the highest summit of the cirque.^c Main aspect of the cirque.^d CRE age showing the deglaciation of the cirque. Note that small glaciers may have remained at the foot of the cirque walls. All ages are related to the bedrock and/or moraines distributed at the mouth of the cirque.^e CRE ages indicating the final deglaciation of the cirque. All ages correspond to bedrock or moraines located in the highest parts of the cirque.^f CRE ages reporting the stabilization of the rock glacier fronts. If there are two ages, the second one corresponds to the stabilization of the roots of the rock glacier.^g Existence of landforms generated by Neoglacial advances with the available CRE ages, if existing.

et al., 2006; Crest et al., 2017; Palacios et al., 2017a; Andrés et al., 2019) and one in the Central Range (Carrasco et al., 2015). However, dating of bedrock surfaces in nine other cirques shows that glaciers occupied the bottom of the cirques until the beginning of the Holocene (CRONUS-Earth Web, Domínguez-Villar et al., 2013, 2012b, 2017a; García-Ruiz et al., 2020a; Crest et al., 2017; Andrés et al., 2019; Jomelli et al., 2020). Although the age of the bedrock surfaces and the moraines resting on them suggest the occurrence of different glacial phases, in this global analysis the mean of the two types of ages can be interpreted as indicative of the final ice disappearance from the cirques. The average age of the deglaciation of all these cirques is 11.2 ka (n = 17), which fits within the onset of the Holocene, once temperatures increased following the YD (Table 4 and Fig. 9A). In the rest of the cirques, there is a lack of information on the glacial impact of the YD due to lack of dating or because the bottoms are still occupied by rock glaciers. According to the 9 cirques with dated moraines, the glaciers in the YD never exceeded the limits of the cirque, with lengths between 500 and 1200 m (Table 4). The abrupt warming after the YD cold period is evidenced in marine and terrestrial records of the regional Iberian context (Fletcher et al., 2010a, 2010b; Moreno et al., 2014; García-Ruiz et al., 2016; López-Sáez et al., 2020).

(iii) In some cases, boulder exposure ages from the front of the rock glaciers are provided. It is assumed that these ages

represent the melting of the interstitial ice, i.e. the stabilization of the rock glacier fronts (Zasadni et al., 2020). In six cirques, rock glaciers likely stabilized somewhat before or at the start of the B-A Interstadial (Rodríguez-Rodríguez et al., 2016, 2017; Andrés et al., 2019; García-Ruiz et al., 2020a), but the roots of the large rock glacier complexes stabilized during the Middle to Late Holocene (Palacios et al., 2017a; Andrés et al., 2019; Jomelli et al., 2020). The stabilization periods (onset, duration and ending) of two debris-covered glaciers from the Iberian Range were determined by the aspect, and hence by solar radiation. They range from the beginning of the B-A to the Middle Holocene (Fernández-Fernández et al., 2017) (Table 4).

- (iv) Neoglacial landforms are located in cirque floors only at the foot of the northern face of peaks above 3000 m in the Central Pyrenees (García-Ruiz et al., 2014, 2020b).
- (v) In summary, in all highest Iberian mountains geomorphological features similar to those in the Sierra Nevada cirques have been observed, regarding both type and development period. The deglaciation of the cirques started at the beginning of the B-A and new glaciers developed during the YD. Following the glacial retreat at the onset of the B-A, as well as during the Early Holocene, shrinking glaciers triggered the formation of rock glaciers in areas of high sediment supply (e.g. at the foot of steep rock walls), with their fronts stabilizing shortly after forming. The sediment supply of the cirques depends on the rock types (see Table 4), but also on the

persistence of weathered substrate of the cirque rock wall, especially in granitic areas (Palacios et al., 2017a; Andrés et al., 2019).

5.4. Diversity of landforms associated with cirque deglaciation in the Northern Hemisphere

In order to explore if the geomorphological evolution within glacial cirques in the Sierra Nevada and other Iberian ranges represents a local or a more widespread climatic pattern, we have examined dozens of glacial cirques in the Northern Hemisphere where CRE data are available (Table 5). To this end, we have analysed chronological data from cirques from the Mediterranean region, Central Europe (Table 6), the British Isles and subpolar regions (Table 7). We have also included the analysis of numerous cirques in

the western United States where precise chronologies are available (Marcott et al., 2019).

- (i) Located between 31 and 37° N, 11 Mediterranean cirques from the Anatolian and Balkan peninsulas and north Morocco benefitting from new detailed CRE chronology were analysed. Eight of the 11 cirques include chronological data on their initial deglaciation. All of them became ice-free at an averaged CRE age of 14.1 ± 1.4 ka ($n = 8$), in consistency with the findings from Iberia (Table 5, Fig. 9B) (Köse et al., 2019; Sarıkaya et al., 2017; Styllas et al., 2018; Hughes et al., 2018; Žebre et al., 2019). Seven cirques include moraine ridges inside the cirques, five of which formed during the YD (Köse et al., 2019; Sarıkaya et al., 2017; Styllas et al., 2018; Hughes et al., 2018; Žebre et al., 2019). Only a few limestone cirques in the Anatolian peninsula reported significantly

Table 8

Location, main topographic characteristics, geomorphological units, and average CRE ages of the cirques studied in the Western North America. All CRE ages are updated.

Cirque/Valley	Massif/range ^a	Elevation (m a.s.l.) and coordinates ^b	Aspect ^c	Deglaciation of the cirque (ka) ^d	Youngest moraine/bedrock (ka) ^e	Distance from headwall to the youngest moraine (m)	Rock glacier landforms (ka) ^f	Neoglacial landforms ^g	References
Little Anapurna/Inspiration Lake	Central Cascades Washington	2660 47°28'8"N 120°48'50"W	NE		10.7 ± 0.6 (n = 5)	1200			Marcott et al. (2019)
Solitude Lake	Teton Range Wyoming	3209 43°48'14"N 110°50'52"W	E		12.8 ± 0.4 (n = 3)	1300			Licciardi and Pierce (2008); Marcott et al. (2019)
Roaring Fork Stough Creek	Wind River Range Wyoming	3720 42°38'2"N 109°1'29"W	NE		12.8 ± 0.7 (n = 4)	700	Proto-rock glacier 9.6 ± 0.5 (n = 7)	Active rock glacier	Marcott et al. (2019)
Temple lake	Wind River Range Wyoming	3953 42°41'55"N 109°10'15"W	NW	14.0 ± 1.0 (n = 7)					Marcott et al. (2019)
Medicine Bow	Rocky Mts, Wyoming	3580 41°20'36"N106°19'51"W	E	14.5 ± 0.7 (n = 6)	11.5 ± 0.7 (n = 6)	600	Proto-rock glacier 10.5 ± 0.6 (n = 6)		Marcott et al. (2019)
Agassiz/Blue Lake	Uinta Mts., Utah	3788 40°42'39"N 110°49'30"W	E	14.4 ± 0.7 (n = 6)					Marcott et al. (2019)
Dead Horse Lake	Uinta Mts., Utah	3650 40°44'24"N 110°40'48"W	NE	13.4 ± 0.7 (n = 6)	11.8 ± 0.6 (n = 6)	600	Proto-rock glacier 10.5 ± 0.5 (n = 6)		Marcott et al. (2019)
Arapahoe Cirque	Colorado Front Range	4115 40°01'35"N 105°39'01"W	E		11.6 ± 0.5 (n = 6)	1800	Inner moraine 10.0 ± 0.6 (n = 6)		Marcott et al. (2019)
Warren Mt. Chicago lakes	Colorado Front Range	4055 39°36'19"N 105°37'59"W	NE	15.2 ± 0.7 (n = 5)					Marcott et al. (2019)
Wheeler	South Snake Range Nevada	3982 38°59'10"N 114°18'48"W	NE		12.5 ± 1.3 (n = 6)	1800		Active rock glacier	Marcott et al. (2019)
Mount Thompson Boon lakes	Sierra Nevada California	4112 37°8'35"N 118°36'48"W	N		12.5 ± 0.8 (n = 5)	2800			Marcott et al. (2019)
Badly/Katherine	Sangre de Cristo Mts, New Mexico.	3840 35°49'57"N105°45'28"W	SE	15.1 ± 0.8 (n = 10)					Marcott et al. (2019)

^a Name of the cirque within the mountain range.

^b Elevation and geographic coordinates of the highest summit of the cirque.

^c Main aspect of the cirque.

^d CRE age showing the deglaciation of the cirque. Note that small glaciers may have remained at the foot of the cirque walls. All ages are related to the bedrock and/or moraines distributed at the mouth of the cirque.

^e CRE ages indicating the final deglaciation of the cirque. All ages correspond to bedrock or moraines located in the highest parts of the cirque.

^f CRE ages reporting the stabilization of the rock glacier fronts. If there are two ages, the second one corresponds to the stabilization of the roots of the rock glacier.

^g Existence of landforms generated by Neoglacial advances with, if existing, the available CRE ages.

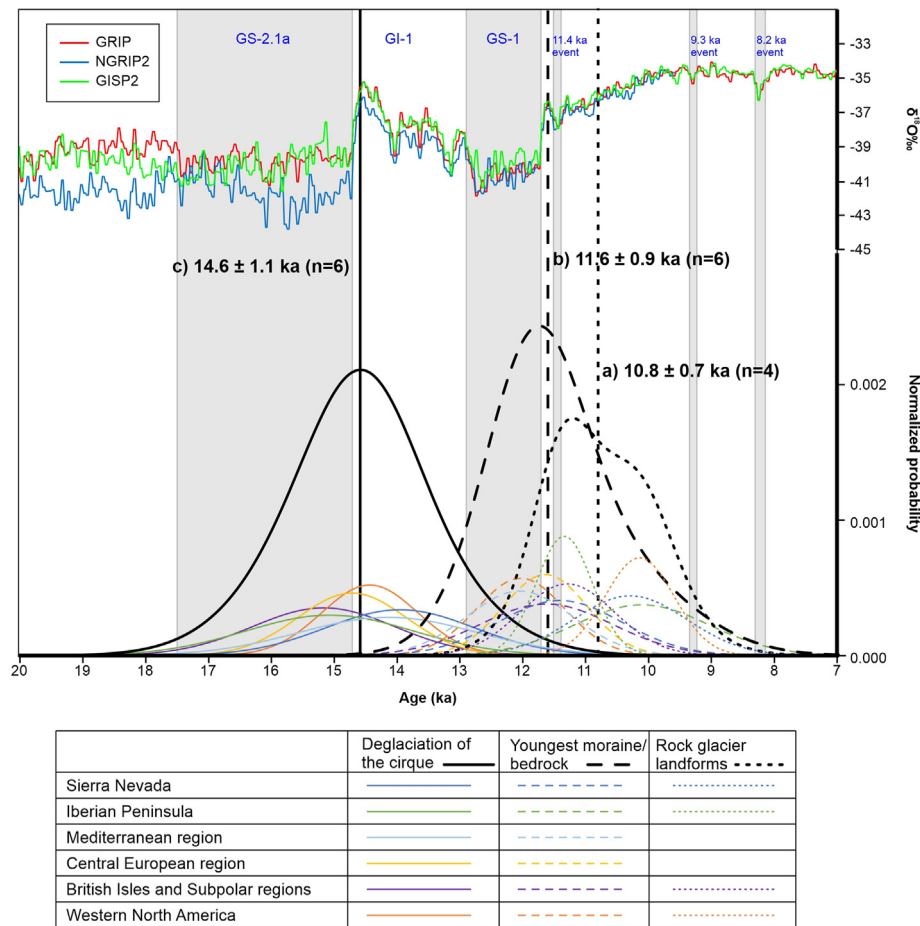


Fig. 10. Probability density plots of CRE ages for different chronostratigraphical units, comparing all the results from the six regions. The plots are clustered in a) Rock glacier front stabilization after the YD; b) Deglaciation of the cirque floor after the YD (ages of the stabilization of the youngest moraine and polished bedrock surfaces); c) Deglaciation of the mouth of the cirque, at the beginning of the B-A Interstadial (ages of the stabilization of the oldest moraine inside the cirque and polished bedrock surfaces). The number associated with each averaged CRE age refers to the number of cirques with available CRE ages in a given region analysed. The average CRE age of each geomorphological unit is compared with the Greenland ice core chronology (Rasmussen et al., 2014).

younger moraine ages (Sarıkaya et al., 2017). With the exception of these excluded cases, the average CRE age of these moraines is 12.0 ± 0.8 ka ($n = 8$) (Table 5, Fig. 9B) and the glacier lengths ranged from 700 to 2500 m. There are only some CRE-dated rock glaciers in this region. Evidencing cosmogenic nuclide inheritance, they were not included in our analysis (Çiner et al., 2017). Neoglacial landforms appear only in cirques with peaks near 3000 m (Styllas et al., 2018), with the exception of Anatolia (Sarıkaya et al., 2017).

- (ii) 17 cirques from Central Europe mountains located between 45° and 50° N were analysed. Most of them are situated in the Carpathian Mountains, only two being low-altitude cirques from the Alps. In the Central Alps, the YD glaciers were beyond the cirque area and, hence, they are not considered in our analysis. Up to 15 cirques include moraines with CRE ages ranging from 15.5 ± 0.4 to 13.2 ± 1.0 ka, leading to an averaged CRE age of 14.7 ± 0.9 ka ($n = 14$) (Table 6, Fig. 9C) (Engel et al., 2014, 2017; Gheorghiu et al., 2015; Makos et al., 2018; Zasadni et al., 2020). Their stabilization might be related to the beginning of the B-A. Only 6 cirques included moraine formation during the YD/Early Holocene transition, whose CRE ages range between 12.0 ± 1.1 and 10.9 ± 0.6 ka, leading to an averaged CRE age of 11.6 ± 0.7 ka ($n = 6$) (Table 6, Fig. 9C) (Engel et al., 2014; Gheorghiu et al., 2015; Makos et al., 2018). The YD glaciers had limited areas, with

lengths between 500 and 800 m. 6 cirques do not host YD moraines, but include rock glaciers, whose fronts stabilized at CRE ages ranging from 12.9 ± 0.7 to 10.9 ± 1.0 ka, also during the YD/Early Holocene transition (Moran et al., 2016; Zasadni et al., 2020) (Table 6). There is no evidence of Neoglacial landforms.

- (iii) Six cirques from the British Isles and three from northern Iceland were analysed. Only three British cirques provide information regarding their initial deglaciation. They became ice-free prior to or during the B-A at an average age of 15.2 ± 1.1 ka ($n = 3$) (Table 7, Fig. 9D) (Barth et al., 2018). Four British and two Icelandic cirques host moraines whose stabilization ages range from 12.0 ± 0.9 to 10.7 ± 1.0 ka, leading to an average age of 11.6 ± 1.1 ka ($n = 6$) (Table 7, Fig. 9D). Therefore, they probably formed during the YD (Barth et al., 2018; Hughes et al., 2019; Fernández-Fernández et al., 2020). The British YD cirque glaciers were between 300 and 950 m long while the Icelandic ones were longer, between 1500 and 3000 m. The stabilization of one rock glacier has been dated in Britain at 12.5 ± 1.1 ka ($n = 5$; Barth et al., 2018) and two others in Iceland lead to a reported average age of 10.1 ± 1.0 ka ($n = 4$; Fernández-Fernández et al., 2020).
- (iv) Until very recently, chronological data about the formation of landforms inside glacial cirques from North America was very limited, but a recent study provides information about

cirques from the Western United States (Marcott et al., 2019). Located between 35° to 47° N, 12 cirques were examined. Six of these cirques provide deglaciation ages based on the chronology of the stabilization of their moraines that occurred during the B-A, their ages between 15.2 ± 0.7 and 13.4 ± 0.7 ka lead to an average age of 14.4 ± 0.8 ka ($n = 6$) (Table 8, Fig. 9E) (Marcott et al., 2019). Eight of the American cirques have internal moraines whose ages between 12.8 ± 0.7 and 10.7 ± 0.6 ka lead to an average age of 12.0 ± 0.7 ka ($n = 8$) likely corresponding to the YD (Table 8, Fig. 9E) (Marcott et al., 2019). These YD glaciers were between 700 and 2800 m long. Three of these cirques have rock glaciers whose ages of stabilization range between 10.5 ± 0.6 and 9.6 ± 0.5 ka (Marcott et al., 2019).

- (v) The comparison of the different deglaciation chronologies and of the development of rock glaciers allows inferring if there is a synchronic pattern across the Northern Hemisphere. The comparison of all the averaged ages of the rock glacier front stabilization reveals that they chronologically coincide with phases following the deglaciation of these cirques, i.e. fifteen of them (average age: 10.8 ± 0.7 ka) after the YD, and 5 of them (average age: 15.4 ± 1.5 ka) with the end of the OD (Tables 3–8 and Fig. 9F). Since most of the analysed cirques were deglaciated after the YD, most of the rock glacier fronts stabilized shortly thereafter, around 1 ka after deglaciation (Palacios et al., 2016, 2017a; Moran et al., 2016; Fernández-Fernández et al., 2020; Marcott et al., 2019; Zasadni et al., 2020).
- (vi) Based on the typology and age of the landforms observed inside the cirques in the mid-latitude mountains of the Northern Hemisphere, we concluded that the geomorphological dynamics of all these cirques were similar to those studied in the Sierra Nevada and in the rest of the Iberian Peninsula. As in the Sierra Nevada, the diversity of geomorphic landforms in each cirque depends on the local topographic characteristics of the altitude of its summits and floors as well as on its orientation and prevailing lithology. However, most of the moraine systems and rock glaciers distributed inside glacial cirques formed during the same climatic phases throughout the Hemisphere, from the Last Termination to the present.

In fact, two distinct geomorphological phases are clearly linked to the warm phases during the Last Termination in the Northern Hemisphere: (i) The glacier margins receded from the mouth of the cirques – generating in many cases moraines (Table 8) – during the climate oscillations of the OD and the B-A transition; (ii) in most cirques, the glaciers expanded or remained during the YD and generated moraines within the limits of the cirques (Fig. 10). These glaciers retreated up-valley and abandoned their moraines at the onset of the Holocene, when rock glacier fronts stabilized (Fig. 10).

6. Conclusions

This work provides robust evidence that glacial cirques reflect the climatic conditions prevailing during their formation (Benedict, 1973; Dahl and Nesje, 1992; Delmas et al., 2015; Barr et al., 2017; Barr and Spagnolo, 2015; Ipsen et al., 2018), and also preserve very valuable information on the climatic and geomorphological evolution that occurred during their deglaciation:

- (i) All the examined cirques were deglaciated during the OD and the B-A transition. There are no geomorphic remnants in none of the examined cirques of the Northern Hemisphere supporting the existence of glaciers during the B-A. Although

survival of glaciers through the B-A in the cirques is fully possible, it is not proven. While glaciers retreated during the OD and B-A transition in many cirques, in others the glaciers evolved into rock glaciers but their fronts stabilized soon after their formation.

- (ii) There is widespread evidence of the existence of glaciers during the YD in many cirques, as shown by: (i) the age of glacier retreat revealed by the age of polished bedrock surfaces, and (ii) the age of moraine boulders stabilization. In both cases, results provide ages spanning the late YD and early Holocene.
- (iii) The retreat of YD glaciers generated a wide variety of landforms within each cirque: (a) Sometimes, after the glaciers disappeared, only polished surfaces remained. This is a widespread pattern in Iberian mountains, and probably in other mid-latitude mountains, although in other regions there are very few studies that have dated bedrock surfaces located at the bottom of the cirques. (b) In other cases, following the melting of glaciers, moraines rapidly stabilized. (c) Moraines did not form in many cirques, but the retreat of YD glaciers favoured the development of rock glaciers. In many cases, their fronts stabilized shortly after their formation, even in less than 1 ka (Zasadni et al., 2020). (d) In other cases, debris-covered glaciers could also form. In fact, many of the analysed rock glaciers may have originated from debris covered glaciers formed in previous phases of the long-term deglaciation process (Anderson et al., 2018). The detailed study conducted on the wide variety of cirques in the Sierra Nevada provided information about the topographical setting that determined every type of evolution. Similar studies should be done in other mountain systems to better determine every single type of geomorphological evolution and infer the role of climate, topography and lithology in their evolution.
- (iv) In most cirques, no major changes have occurred on geomorphological dynamics since the HTM. Landscapes have only undergone minor transformations related to periglacial and slope processes. Neoglacial landforms only developed in the highest mountains, such as in the case of the Sierra Nevada, where glaciers developed in cirques with summits exceeding 3300 m. The diversity of cirque landforms depends on local conditions and, above all, on the geomorphological activity of their headwalls. In some cases, the retreat of small Neoglacial ice masses triggered the formation of incipient rock glaciers.
- (v) This study highlights that the formation of rock glaciers inside the cirques is triggered by the onset of warm phases that accelerate the retreat of glaciers. Therefore, they are more associated with the paraglacial readjustment following glacial retreat (Ballantyne, 2002) rather than with a periglacial origin driven by very cold temperatures. This explains the rapid stabilization of their fronts once the internal frozen body disappears (Gómez-Ortiz et al., 2014).

Glacial cirques have been shown to be highly climatically sensitive areas where small changes favoured the development or disappearance of glaciers. In addition, the activity of their walls is critical to generate a great variety of landforms, depending on their topographic characteristics. Glacial cirques are, therefore, a valuable source of palaeoenvironmental information to better understand the landscape evolution of mountain systems since the last deglaciation to recent times.

Author statement

The investigation has been carried out by the following authors, who have been involved in the following tasks: David Palacios: coordination of the entire research, fieldwork, sampling, data processing, interpretation of the results and writing the first draft of the manuscript. Review of all work according to the comments of the reviewers. Marc Oliva: fieldwork, sampling, data processing and collaboration in the writing. Review of all work according to the comments of the reviewers. Antonio Gomez-Ortiz: fieldwork, sampling, data interpretation and collaboration in the writing. Review of all work according to the comments of the reviewers. Nuria Andrés: data processing, geomorphological mapping and collaboration in the writing. Review of all work according to the comments of the reviewers. José M. Fernández-Fernández: data processing, geomorphological mapping and collaboration in the writing. Review of all work according to the comments of the reviewers. Irene Schimmelpfennig: Supervision of the whole process of sample processing, interpretation of the results and correction of the manuscript. Review of all work according to the comments of the reviewers. Laëticia Léanni: sample processing in laboratory, Supervision of AMS measurements and correction of the manuscript. Review of all work according to the comments of the reviewers. ASTER Team: Supervision of AMS measurements and correction of the manuscript. Review of all work according to the comments of the reviewers.

Declaration of competing interest

The authors declare that they have no known competing financial interests or personal relationships that could have appeared to influence the work reported in this paper.

Acknowledgements

This research article was supported by the project CGL2015-65813-R (Spanish Ministry of Economy and Competitiveness) and NUNANTAR (02/SAICT/2017–32002; Fundação para a Ciência e a Tecnologia, Portugal). It also complements the research topics examined in the project PALAEOGREEN (CTM2017-87976-P; Spanish Ministry of Economy and Competitiveness). The ^{10}Be measurements were performed at the ASTER AMS national facility (CEREGE, Aix-en-Provence), which is supported by the INSU/ CNRS and the ANR through the “Projets thématiques d'excellence” program for the “Equipements d'excellence” ASTER-CEREGE action and IRD. Marc Oliva is supported by the Ramón y Cajal Program (RYC-2015-17597) and the Research Group ANTALP (Antarctic, Arctic, Alpine Environments; 2017-SGR-1102). The authors are deeply appreciative for the detailed analyses and excellent suggestions made by the two reviewers, Drs. Ian Evans and Philip Hughes, who helped to considerably improve many aspects of this work.

Appendix A. Supplementary data

Supplementary data associated with this article can be found, in the online version, at <https://doi.org/10.1016/j.quascirev.2020.106617>.

References

- Anderson, R.S., Anderson, L.S., Armstrong, W.H., Rossi, M.W., Crump, S.E., 2018. Glaciation of alpine valleys: the glacier–debris-covered glacier–rock glacier continuum. *Geomorphology* 311, 127–142. <https://doi.org/10.1016/j.geomorph.2018.03.015>.
- Anderson, R.S., Jiménez-Moreno, G., Carrión, J.S., Pérez-Martínez, C., 2011. Post-glacial history of alpine vegetation, fire, and climate from Laguna de Río Seco,

- Sierra Nevada, southern Spain. *Quat. Sci. Rev.* 30, 1615–1629. <https://doi.org/10.1016/j.quascirev.2011.03.005>.
- Andrés, N., Gómez-Ortiz, A., Fernández-Fernández, J.M., Tanarro, L.M., Salvador, F., Oliva, M., Palacios, D., 2019. Timing of deglaciation and rock glacier origin in the southeastern Pyrenees: a review and new data. *Boreas* 47, 1050–1071. <https://doi.org/10.1111/bor.12324>.
- Arnold, M., Merchel, S., Bourlès, D.L., Braucher, R., Benedetti, L., Finkel, R.C., Aumaitre, G., Gottsdang, A., Klein, M., 2010. The French accelerator mass spectrometry facility ASTER: improved performance and developments. *Nuclear Instruments and Methods in Physics Research, Section B, Beam Interactions with Materials and Atoms*, 19th International Conference on Ion Beam Analysis 268, 1954–1959. <https://doi.org/10.1016/j.nimb.2010.02.107>.
- Ballantyne, C.K., 2002. Paraglacial geomorphology. *Quat. Sci. Rev.* 21, 1935–2017. [https://doi.org/10.1016/S0277-3791\(02\)00005-7](https://doi.org/10.1016/S0277-3791(02)00005-7).
- Ballantyne, C.K., 2013. Paraglacial geomorphology. *Encyclopedia of Quaternary Science*, second ed. Elsevier, pp. 553–565. <https://doi.org/10.1016/B978-0-444-53643-3.00089-3>.
- Baroni, C., Guidobaldi, G., Salvatore, M.C., Christl, M., Ivy-Ochs, S., 2018. Last glacial maximum glaciers in the Northern Apennines reflect primarily the influence of southerly storm-tracks in the western Mediterranean. *Quat. Sci. Rev.* 197, 352–367. <https://doi.org/10.1016/j.quascirev.2018.07.003>.
- Barr, I.D., Spagnolo, M., 2015. Glacial cirques as palaeoenvironmental indicators: their potential and limitations. *Earth Sci. Rev.* 151, 48–78. <https://doi.org/10.1016/j.earscirev.2015.10.004>.
- Barr, I.D., Ely, J.C., Spagnolo, M., Clark, C.D., Evans, I.S., Pellicer, X.M., et al., 2017. Climate patterns during former periods of mountain glaciation in Britain and Ireland: inferences from the cirque record. *Palaeogeogr. Palaeoclimatol. Palaeoecol.* 485, 466–475. <https://doi.org/10.1016/j.palaeo.2017.07.001>.
- Barth, A.M., Clark, P.U., Clark, J., McCabe, A.M., Caffee, M., 2016. Last glacial maximum cirque glaciation in Ireland and implications for reconstructions of the Irish ice sheet. *Quat. Sci. Rev.* 141, 85–93. <https://doi.org/10.1016/j.quascirev.2016.04.006>.
- Barth, A.M., Clark, P.U., Clark, J., Roe, G.H., Marcott, S.A., McCabe, A.M., et al., 2018. Persistent millennial-scale glacier fluctuations in Ireland between 24 ka and 10 ka. *Geology* 46 (2), 151–154. <https://doi.org/10.1130/G39796.1>.
- Benedict, J.B., 1973. Chronology of cirque glaciation, Colorado front range. *Quat. Res.* 3 (4), 584–599.
- Benn, D.I., Evans, D.J.A., 2010. *Glaciers and Glaciation*. Hodder Education, London.
- Braucher, R., Guillou, V., Bourlès, D.L., Arnold, M., Aumaitre, G., Keddadouche, K., Nottoli, E., 2015. Preparation of ASTER in-house $^{10}\text{Be}/^9\text{Be}$ standard solutions. Nuclear instruments and methods in physics research, section B, beam interactions with materials and atoms. The Thirteenth Accelerator Mass Spectrometry Conference 361, 335–340. <https://doi.org/10.1016/j.nimb.2015.06.012>.
- Carrasco, R.M., Pedraza, J., Dominguez-Villar, D., Willenbring, J.K., Villa, J., 2013. Supraglacial debris supply in the Cuerpo de Hombre palaeoglacier (Spanish Central System). Reconstruction and interpretation of a rock avalanche event. *Geogr. Ann. Ser. A Phys. Geogr.* 95, 211–266. <https://doi.org/10.1111/geoa.12010>.
- Carrasco, R.M., Pedraza, J., Dominguez-Villar, D., Willenbring, J.K., Villa, J., 2015. Sequence and chronology of the Cuerpo de Hombre palaeoglacier (Iberian Central System) during the last glacial cycle. *Quat. Sci. Rev.* 129, 163–177. <https://doi.org/10.1016/j.quascirev.2015.09.021>.
- Carrasco, R.M., Pedraza, J., Willenbring, J., Karampaglidis, T., Soteres, R.L., Martín-Duque, J.F., 2016. Morfología glacial del Macizo de Los Pelados-El Nevero (Parque Nacional de la Sierra de Guadarrama). Nueva interpretación y cronología. *Bol. R. Soc. Esp. Hist. Nat. Sec. Geol.* 110, 49–66.
- Çiner, A., Sarikaya, M.A., Yildirim, C., 2017. Misleading old age on a young landform? The dilemma of cosmogenic inheritance in surface exposure dating: moraines vs. rock glaciers. *Quat. Geochronol.* 42, 76–88. <https://doi.org/10.1016/j.quageo.2017.07.003>.
- Chmieleff, J., von Blanckenburg, F., Kossert, K., Jakob, D., 2010. Determination of the ^{10}Be half-life by multicollector ICP-MS and liquid scintillation counting. *Nucl. Instrum. Methods Phys. Res. Sect. B Beam Interact. Mater. Atoms* 268, 192–199. <https://doi.org/10.1016/j.nimb.2009.09.012>.
- Clark, D.H., Gillespie, A.R., 1997. Timing and significance of late-glacial and Holocene cirque glaciation in the Sierra Nevada, California. *Quat. Int.* 38, 21–38. [https://doi.org/10.1016/S1040-6182\(96\)00024-9](https://doi.org/10.1016/S1040-6182(96)00024-9).
- Clark, P.U., Dyke, A.S., Shakun, J.D., Carlson, A.E., Clark, J., Wohlfarth, B., Mitrovica, J.X., Hostetler, S.W., McCabe, A., 2009. The last glacial maximum. *Science* 325, 710–714. <https://doi.org/10.1126/science.1172873>.
- Crest, Y., Delmas, M., Braucher, R., Gunnell, Y., Calvet, M., Aster Team, 2017. Cirques have growth spurts during deglacial and interglacial periods: evidence from ^{10}Be and ^{26}Al nuclide inventories in the central and eastern Pyrenees. *Geomorphology* 278, 60–77. <https://doi.org/10.1016/j.geomorph.2016.10.035>.
- CRONUS-Earth Web Calculators v2.0 2020: Available at: <http://cronus.cosmogenicnuclides.rocks/2.0/html/topo/> (accessed March 2020).
- Dahl, S.O., Nesje, A., 1992. Palaeoclimatic implications based on equilibrium-line altitude depressions of reconstructed Younger Dryas and Holocene cirque glaciers in inner Nordfjord, western Norway. *Palaeogeogr. Palaeoclimatol. Palaeoecol.* 94 (1–4), 87–97. [https://doi.org/10.1016/0031-0182\(92\)90114-K](https://doi.org/10.1016/0031-0182(92)90114-K).
- Deline, P., Akçar, N., Ivy-Ochs, S., Kubik, P.V., 2015. Repeated holocene rock avalanches onto the Brenva glacier, mont blanc massif, Italy: a chronology. *Quat. Sci. Rev.* 126, 186–200. <https://doi.org/10.1016/j.quascirev.2015.09.004>.
- Delmas, M., 2015. The last maximum ice extent and subsequent deglaciation of the Pyrenees: an overview of recent research. *Cuadernos de Investigación Geográfica* 41 (2), 359–387. <https://doi.org/10.18172/cig.2708>.

- Delmas, M., Gunnell, Y., Calvet, M., 2015. A critical appraisal of allometric growth among alpine cirques based on multivariate statistics and spatial analysis. *Geomorphology* 228, 637–652. <https://doi.org/10.1016/j.geomorph.2014.10.021>.
- Dominguez-Villar, D., Carrasco, R.M., Pedraza, J., Cheng, H., Edwards, R.L., Willenbring, J.K., 2013. Early maximum extent of palaeoglaciators from Mediterranean mountains during the last glaciation. *Sci. Rep.* 3, 2034. <https://doi.org/10.1038/srep02034>.
- Engel, Z., Braucher, R., Traczyk, A., Laetitia, L., 2014. ¹⁰Be exposure age chronology of the last glaciation in the Krkonoše Mountains, Central Europe. *Geomorphology* 206, 107–121. <https://doi.org/10.1016/j.geomorph.2013.10.003>.
- Engel, Z., Mentlik, P., Braucher, R., Minár, J., Léanni, L., Aster Team, 2015. Geomorphological evidence and ¹⁰Be exposure ages for the last glacial maximum and deglaciation of the veľká and malá studená dolina valleys in the high Tatras mountains, central Europe. *Quat. Sci. Rev.* 124, 106–123. <https://doi.org/10.1016/j.quascirev.2015.07.015>.
- Evans, I.S., Cox, N.J., 1974. Geomorphometry and the operational definition of cirques. *Area* 6, 150–153.
- Evans, I.S., Cox, N.J., 1995. The form of glacial cirques in the English Lake District, Cumbria. *Z. Geomorphol.* 39, 175–202.
- Fernández-Fernández, J.M., Palacios, D., García-Ruiz, J.M., Andrés, N., Schimmelpfennig, I., Gómez-Villar, A., Santos González, J., Álvarez-Martínez, J., Arnáez, J., Úbeda, J., Léanni, L., ASTER Team, 2017. Chronological and geomorphological investigation of fossil debris-covered glaciers in relation to deglaciation processes: a case study in the Sierra de la Demanda, northern Spain. *Quat. Sci. Rev.* 170, 232–249. <https://doi.org/10.1016/j.quascirev.2017.06.034>.
- Fernández-Fernández, J.M., Palacios, D., Andrés, N., Schimmelpfennig, I., Brynjólfsson, S., Sancho, L.G., Zamorano, J.J., Heiðmarsson, S., Sæmundsson, Þ., ASTER Team, 2019. A multi-proxy approach to Late Holocene fluctuations of Tungnahryggssjökull glaciers in the Tröllaskagi peninsula (northern Iceland). *Sci. Total Environ.* 664, 499–517. <https://doi.org/10.1016/j.scitotenv.2019.01.364>. Citations: 1.
- Fernández-Fernández, J.M., Palacios, D., Andrés, N., Schimmelpfennig, I., Tanarro, L.M., Brynjólfsson, S., López-Acevedo, F.J., Sæmundsson, Þ., Team, A.S.T.E.R., 2020. Constraints on the timing of debris-covered and rock glaciers: an exploratory case study in the Hólar area, northern Iceland. *Geomorphology* 361, 107196. <https://doi.org/10.1016/j.geomorph.2020.107196>.
- Fletcher, W.J., Sánchez Goñi, M.F., Allen, J.R.M., Cheddadi, R., Cambourieu-Nebout, N., Huntley, B., Lawson, I., Londeix, L., Magri, D., Margari, V., Müller, U.C., Naughton, F., Novenko, E., Roucoux, K., Tzedakis, P.C., 2010a. Millennial-scale variability during the last glacial in vegetation records from Europe. *Quat. Sci. Rev.* 29 (21–22), 2839–2864. <https://doi.org/10.1016/j.quascirev.2009.11.015>.
- Fletcher, W.J., Sánchez-Goñi, M.F., Peyron, O., Dormoy, I., 2010b. Abrupt climate changes of the last deglaciation. Western Mediterranean forest record. *Clim. Past* 6, 245–264. <https://doi.org/10.5194/cp-6-245-2010>.
- García-Alix, A., Jiménez-Espejo, F.J., Lozano, J.A., Jiménez-Moreno, G., Martínez-Ruiz, F., García Sanjuán, L., Aranda Jiménez, G., García Alfonso, E., Ruiz-Puertas, G., Anderson, R.S., 2013. Anthropogenic impact and lead pollution throughout the holocene in southern Iberia. *Sci. Total Environ.* 449, 451–460. <https://doi.org/10.1016/j.scitotenv.2013.01.081>.
- García-Alix, A., Jiménez-Espejo, F.J., Toney, J.L., Jiménez-Moreno, G., Ramos-Román, M.J., Anderson, R.S., Ruano, P., Queralt, I., Delgado Huertas, A., Kuroda, J., 2017. Alpine bogs of southern Spain show human-induced environmental change superimposed on long-term natural variations. *Sci. Rep.* 7, 1–12. <https://doi.org/10.1038/s41598-017-07854-w>.
- García-Ruiz, J.M., Palacios, D., de Andrés, N., Valero-Garcés, B.L., López-Moreno, J.I., Sanjuán, Y., 2014. Holocene and 'little ice age' glacial activity in the Marboré cirque, Monte Perdido massif, central Spanish Pyrenees. *Holocene* 24 (11), 1439–1452. <https://doi.org/10.1177/0959583614544053>.
- García-Ruiz, J.M., Palacios, D., González-Sampériz, P., De Andrés, N., Moreno, A., Valero-Garcés, B., Gómez-Villar, A., 2016. Mountain glacier evolution in the Iberian peninsula during the younger Dryas. *Quat. Sci. Rev.* 138, 16–30. <https://doi.org/10.1016/j.quascirev.2016.02.022>.
- García-Ruiz, J.M., Palacios, D., Fernández-Fernández, J.M., Andrés, N., Arnáez, J., Gómez-Villar, A., Santos-González, J., Álvarez-Martínez, J., Lana-Renault, N., Léanni, L., Aster, Team, 2020a. Glacial Stages in the Peña Negra Valley, Iberian Range, Northern Iberian Peninsula: Assessing the Importance of the Glacial Record in Small Cirques in a Marginal Mountain Area. *Geomorphology* (revision).
- García-Ruiz, J.M., Palacios, D., Andrés, N., López-Moreno, J.I., 2020b. Neoglaciation in the Spanish Pyrenees: a multiproxy challenge. *Mediterranean Geoscience Reviews*. <https://doi.org/10.1007/s42990-020-00022-9>.
- Gheorghiu, D.M., Hosu, M., Corpade, C., Xu, S., 2015. Deglaciation constraints in the Parâng Mountains, Southern Romania, using surface exposure dating. *Quat. Int.* 388, 156–167. <https://doi.org/10.1016/j.quaint.2015.04.059>.
- Giraudi, C., 2012. The campo felice late pleistocene glaciation (Apennines, Central Italy). *J. Quat. Sci.* 27, 432e440. <https://doi.org/10.1002/jqs.1569>.
- Gómez-Ortiz, A., Palacios, D., Schulte, L., Salvador-Franch, F., Plana-Castellví, J.A., 2009. Evidences from historical documents of landscape evolution after little ice age of a mediterranean high mountain area, Sierra Nevada, Spain (eighteenth to twentieth centuries). *Geogr. Ann. Ser. A Phys. Geogr.* 91, 279–289. <https://doi.org/10.1111/j.1468-0459.2009.00370.x>.
- Gómez-Ortiz, A., Oliva, M., Salvador-Franch, F., Salvà-Catarineu, M., Plana-Castellví, J.A., 2018. The geographical interest of historical documents to interpret the scientific evolution of the glacier existing in the Veleta cirque (Sierra Nevada, Spain) during the Little Ice Age. *Cuadernos de Investigación Geográfica* 44, 267–292.
- Gómez-Ortiz, A., Oliva, M., Salvador-Franch, F., Palacios, D., Tanarro, L.M., Sanjosé-Blasco, J.J., Salvà-Catarineu, M., 2019. Monitoring permafrost and periglacial processes in Sierra Nevada (Spain) from 2001 to 2016. *Permafrost. Periglac. Process.* <https://doi.org/10.1002/PPP.2002>.
- Gómez-Ortiz, A., Oliva, M., Palacios, D., Salvador-Franch, F., Vázquez-Selem, L., Salvà-Catarineu, M., De Andrés, N., 2015. The deglaciation of Sierra Nevada (Spain), synthesis of the knowledge and new contributions. *Cuadernos Invest. Geogr.* 41, 409. <https://doi.org/10.18172/cig.2722>.
- Gómez-Ortiz, A., Palacios, D., Palade, B., Vázquez-Selem, L., Salvador-Franch, F., 2012. The deglaciation of the Sierra Nevada (southern Spain). *Geomorphology* 159–160, 93–105. <https://doi.org/10.1016/j.geomorph.2012.03.008>.
- Hippolyte, J.C., Bourlès, D., Braucher, R., Carcaillet, J., Léanni, L., Arnold, M., Aumaitre, G., 2009. Cosmogenic ¹⁰Be dating of a sacking and its faulted rock glaciers, in the Alps of Savoy (France). *Geomorphology* 108, 312–320. <http://www.springer.com/us/book/9783642800955>.
- Hughes, P.D., Woodward, J.C., Gibbard, P.L., Macklin, M.G., Gilmour, M.A., Smith, G.R., 2006. The glacial history of the Pindus Mountains, Greece. *J. Geol.* 114, 413–434. <https://doi.org/10.1086/504177>.
- Hughes, P.D., Gibbard, P.L., Woodward, J.C., 2007. Geological controls on Pleistocene glaciation and cirque form in Greece. *Geomorphology* 88 (3), 242–253. <https://doi.org/10.1016/j.geomorph.2006.11.008>.
- Hughes, P.D., Gibbard, P.L., Ehlers, J., 2013. Timing of glaciation during the last glacial cycle: evaluating the concept of a global 'Last Glacial Maximum' (LGM). *Earth Sci. Rev.* 125, 171–198. <https://doi.org/10.1016/j.earscirev.2013.07.003>.
- Hughes, P.D., Fink, D., Rodés, Á., Fenton, C.R., Fujioka, T., 2016. Timing of pleistocene glaciations in the high Atlas, Morocco: new ¹⁰Be and ³⁶Cl exposure ages. *Quat. Sci. Rev.* 180, 193–213. <https://doi.org/10.1016/j.quascirev.2017.11.015>.
- Hughes, P.D., Gibbard, P.L., 2018. Global glacier dynamics during 100 ka Pleistocene glacial cycles. *Quat. Res.* 90 (1), 222–243. <https://doi.org/10.1017/qua.2018.37>.
- Hughes, P.D., Tomkins, M.D., Stimson, G.A., 2019. Glaciation of the English Lake District during the Late-glacial: a new analysis using ¹⁰Be and Schmidt hammer exposure dating. *North West Geography* 19 (2), 8–20.
- Ipsen, H.A., Principato, S.M., Grube, R.E., Lee, J.F., 2018. Spatial analysis of cirques from three regions of Iceland: implications for cirque formation and palaeoclimate. *Boreas* 47, 565–576. <https://doi.org/10.1111/bor.12295>.
- Ivy-Ochs, S., Kerschner, H., Maisch, M., Christl, M., Kubik, P.W., Schlüchter, C., 2009. Latest pleistocene and Holocene glacier variations in the European Alps. *Quat. Sci. Rev.* 28, 2137–2149. <https://doi.org/10.1016/j.quascirev.2009.03.009>.
- Ivy-Ochs, S., 2015. Glacier variations in the European Alps at the end of the last glaciation. *Cuadernos de Investigación Geográfica* 41 (2), 295–315. <https://doi.org/10.18172/cig.2750>.
- Jiménez-Moreno, G., Anderson, R.S., 2012. Holocene vegetation and climate change recorded in alpine bog sediments from the Borreguiles de la Virgen, Sierra Nevada, southern Spain. *Quat. Res.* 77, 44–53. <https://doi.org/10.1016/j.yqres.2011.09.006>.
- Jomelli, V., Chapron, E., Favier, V., Rinterknecht, V., Braucher, R., Tournier, N., Gascoin, S., Marti, R., Galop, D., Binet, S., Deschamps-Berger, C., Tissoux, H., ASTER Team, 2020. Glacier fluctuations during the Late Glacial and Holocene on the Ariège valley, northern slope of the Pyrenees and reconstructed climatic conditions. *Mediterranean. Geosci. Rev.* 1–15. <https://doi.org/10.1007/s42990-020-00018-5>.
- Kleman, J., Stroeven, A.P., 1997. Preglacial surface remnants and Quaternary glacial regimes in northwestern Sweden. *Geomorphology* 19 (1), 35–54. [https://doi.org/10.1016/S0169-555X\(96\)00046-3](https://doi.org/10.1016/S0169-555X(96)00046-3).
- Knight, J., Harrison, S., Jones, D.B., 2018. Rock glaciers and the geomorphological evolution of deglaciating mountains. *Geomorphology* 311, 127–142. <https://doi.org/10.1016/j.geomorph.2018.09.020>.
- Korschinek, G., Bergmaier, A., Faestermann, T., Gerstmann, U.C., Knie, K., Rugel, G., Wallner, A., Dillmann, I., Dollinger, G., von Gostomski, C.L., Kossert, K., Maiti, M., Poutivsev, M., Remmert, A., 2010. A new value for the half-life of ¹⁰Be by Heavy-Ion Elastic Recoil Detection and liquid scintillation counting. *Nucl. Instrum. Methods Phys. Res. Sect. B Beam Interact. Mater. Atoms* 268, 187–191. <https://doi.org/10.1016/j.nimb.2009.09.020>.
- Köse, O., Sarikaya, M.A., Çiner, A., Candaş, A., 2019. Late Quaternary glaciations and cosmogenic ³⁶Cl geochronology of Mount Dedegöl, south-west Turkey. *J. Quat. Sci.* 34 (1), 51–63. <https://doi.org/10.1002/jqs.3080>.
- Kuhlemann, J., Gachev, E., Gikov, A., Nedkov, S., Krumrei, I., Kubik, P., 2013. Glaciation in the Rila Mountains (Bulgaria) during the last glacial maximum. *Quat. Int.* 293, 51–62. <https://doi.org/10.1016/j.quaint.2012.06.027>.
- Laabs, B.J., Licciardi, J.M., Leonard, E.M., Munroe, J.S., Marchetti, D.W., 2020. Updated cosmogenic chronologies of Pleistocene mountain glaciation in the western United States and associated palaeoclimate inferences. *Quat. Sci. Rev.* 242, 106427. <https://doi.org/10.1016/j.quascirev.2020.106427>.
- Le Roy, M., Deline, P., Carcaillet, J., Schimmelpfennig, I., Ermini, M., ASTER Team, 2017. ¹⁰Be exposure dating of the timing of Neoglacial glacier advances in the Ecrins-Pelvoux massif, southern French Alps. *Quat. Sci. Rev.* 178, 118–138. <https://doi.org/10.1016/j.quascirev.2017.10.010>.
- Li, Y., Li, Y., Harbor, J., Liu, G., Yi, C., Caffee, M.W., 2016. Cosmogenic ¹⁰Be constraints on little ice age glacial advances in the eastern tian Shan, China. *Quat. Sci. Rev.* 138, 105–118. <https://doi.org/10.1016/j.quascirev.2016.02.023>.
- Licciardi, J.M., Pierce, K.L., 2008. Cosmogenic exposure-age chronologies of pinedale and bull lake glaciations in greater Yellowstone and the teton range, USA. *Quat. Sci. Rev.* 27 (7–8), 814–831. <https://doi.org/10.1016/j.quascirev.2007.12.005>.

- Lifton, N., Sato, T., Dunai, T.J., 2014. Scaling in situ cosmogenic nuclide production rates using analytical approximations to atmospheric cosmic-ray fluxes. *Earth Planet. Sci. Lett.* 386, 149–160. <https://doi.org/10.1016/j.epsl.2013.10.052>.
- López-Sáez, J.A., Carrasco, R.M., Turu, V., Ruiz-Zapata, B., Gil-García, M.J., Luelmo-Lautenschlaeger, R., et al., 2020. Late Glacial-early holocene vegetation and environmental changes in the western Iberian Central System inferred from a key site: the Navamuno record, Béjar range (Spain). *Quat. Sci. Rev.* 230, 106167. <https://doi.org/10.1016/j.quascirev.2020.106167>.
- Makos, M., Rinterknecht, V., Braucher, R., Toloczko-Pasek, A., Arnold, M., Aumaître, G., et al., 2018. Last glacial maximum and lateglacial in the polish high Tatra mountains-revised deglaciation chronology based on the ^{10}Be exposure age dating. *Quat. Sci. Rev.* 187, 130–156. <https://doi.org/10.1016/j.quascirev.2018.03.006>.
- Mangerud, J.A.N., Landvik, J.Y., 2007. Younger Dryas cirque glaciers in western spitsbergen: smaller than during the little ice age. *Boreas* 36 (3), 278–285. <https://doi.org/10.1080/03009480601134827>.
- Manzano, S., Carrión, J.S., López-Merino, L., Jiménez-Moreno, G., Toney, J.L., Armstrong, H., Anderson, R.S., García-Alix, A., Pérez, J.L.G., Sánchez-Mata, D., 2019. A palaeoecological approach to understanding the past and present of Sierra Nevada, a Southwestern European biodiversity hotspot. *Global Planet. Change* 175, 238–250. <https://doi.org/10.1016/j.gloplacha.2019.02.006>.
- Martin, L., Bland, P.-H., Balco, G., Lave, J., Delunel, R., Lifton, N., Laurent, V., 2017. The CREP program and the ICE-D production rate calibration database: a fully parameterizable and updated online tool to compute cosmic-ray exposure ages. *Quat. Geochronol.* 38, 25–49. <https://doi.org/10.1016/j.quageo.2016.11.006>.
- Marcott, S.A., Clark, P.U., Shakun, J.D., Brook, E.J., Davis, P.T., Caffee, M.W., 2019. ^{10}Be age constraints on latest Pleistocene and Holocene cirque glaciation across the western United States. *Clim. Atmos. Sci.* 2 (5) <https://doi.org/10.1038/s41612-019-0062-z>.
- Mercier, D., Coquin, J., Feuillet, T., Decaulne, A., Cossart, E., Jónsson, H.P., Sæmundsson, P., 2017. Are Icelandic rock-slope failures paraglacial? Age evaluation of seventeen rock-slope failures in the Skagafjörður area, based on geomorphological stacking, radiocarbon dating and tephrochronology. *Geomorphology* 296, 45–58. <https://doi.org/10.1016/j.geomorph.2017.08.011>.
- Merchel, S., Herpers, U., 1999. An update on radiochemical separation techniques for the determination of long-lived radionuclides via accelerator mass spectrometry. *Radiochim. Acta* 84 (4), 215–220. <https://doi.org/10.1524/ract.1999.84.4.215>.
- Merchel, S., Arnold, M., Aumaître, G., Benedetti, L., Bourlès, D.L., Braucher, R., Alfimov, V., Freeman, S.P.H.T., Steier, P., Wallner, A., 2008. Towards more precise ^{10}Be and ^{36}Cl data from measurements at the 10–14 level: influence of sample preparation. *Nucl. Instrum. Methods Phys. Res. Sect. B Beam Interact. Mater. Atoms* 266, 4921–4926. <https://doi.org/10.1016/j.nimb.2008.07.031>.
- Mindrescu, M., Evans, I.S., 2014. Cirque form and development in Romania: allometry and the buzzsaw hypothesis. *Geomorphology* 208, 117–136. <https://doi.org/10.1016/j.geomorph.2013.11.019>.
- Moran, A.P., Ivy-Ochs, S., Vockenhuber, C., Kerschner, H., 2016. Rock glacier development in the northern calcareous Alps at the pleistocene-holocene boundary. *Geomorphology* 273, 178–188. <https://doi.org/10.1016/j.geomorph.2016.08.017>.
- Moreno, A., Svensson, A., Brooks, S.J., Connor, S., Engels, S., Fletcher, W., Genty, D., Heiri, O., Labuhn, I., Persoiu, A., Peyron, O., Sadori, L., Valero-Garcés, B., Wulfs, S., Zanchetta, G., 2014. A compilation of Western European terrestrial records 60–8 ka BP: towards an understanding of latitudinal climatic gradients. *Quat. Sci. Rev.* 106, 167–185. <https://doi.org/10.1016/j.quascirev.2014.06.030>.
- Oliva, M., Schulte, L., Gómez-Ortiz, A., 2008. Solifluction lobes in Sierra Nevada (southern Spain): morphometry and palaeoenvironmental changes. *Proc. Ninth Int. Conf. Permafrost*, 1321–1326.
- Oliva, M., 2009. Holocene Alpine Environments in Sierra Nevada (Southern Spain). University of Barcelona.
- Oliva, M., Gómez-Ortiz, A., Schulte, L., 2010. Tendencia a la aridez en Sierra Nevada desde el holoceno medio inferida a partir de sedimentos lacustres. *Increasing Arid. Sierra Nevada since Mid-Holocene inferred from lake sediments. Boletín de la Asociación de Geógrafos Españoles* (52), 27–42.
- Oliva, M., Schulte, L., Ortiz, A.G., 2011. The role of aridification in constraining the elevation range of Holocene solifluction processes and associated landforms in the periglacial belt of the Sierra Nevada (southern Spain). *Earth Surf. Process. Landforms* 36, 1279–1291. <https://doi.org/10.1002/esp.2116>.
- Oliva, M., Gómez-Ortiz, A., 2012. Late-Holocene environmental dynamics and climate variability in a Mediterranean high mountain environment (Sierra Nevada, Spain) inferred from lake sediments and historical sources. *Holocene* 22, 915–927. <https://doi.org/10.1177/0959683611434235>.
- Oliva, M., Gómez-Ortiz, A., Salvador, F., Ramos, M., Palacios, D., Pereira, P., 2016. Inexistence of permafrost at the Veleta peak (Sierra Nevada). *Sci. Total Environ.* 550, 484–494. <https://doi.org/10.1016/j.scitotenv.2016.01.150>.
- Oliva, M., Zebre, M., Guglielmin, M., Hughes, P.D., Ciner, A., Vieira, G., Bodin, X., Andrés, N., Colucci, R.R., García-Hernández, C., Mora, C., Nofre, J., Palacios, D., Pérez-Alberti, A., Ribolini, A., Ruiz-Fernández, J., Sarikaya, M.A., Serrano, E., Urdea, P., Valcárcel, M., Woodward, J.C., Yıldırım, C., 2018. Permafrost conditions in the mediterranean region since the last glaciation. *Earth Sci. Rev.* 185, 397–436. <https://doi.org/10.1016/j.earscirev.2018.06.018>.
- Oliva, M., Palacios, D., Fernández-Fernández, J.M., Rodríguez-Rodríguez, L., García-Ruiz, J.M., Andrés, N., Carrasco, R.M., Pedraza, J., Pérez-Alberti, A., Valcárcel, M., Hughes, P.D., 2019. Late quaternary glacial phases in the iberian peninsula. *Earth Sci. Rev.* 192, 564–600. <https://doi.org/10.1016/j.earscirev.2019.03.015>.
- Oliva, M., Gómez-Ortiz, A., Vidal, J., Salvador-Franch, F., Salvà-Catarineu, M., 2015. El martillo de Schmidt como un instrumento de datación relativa. Aplicación preliminar a los arcos morrénicos del Corral del Veleta y Hoya del Mulhacén (Sierra Nevada). In: Gómez-Ortiz, A., Salvador-Franch, F., Oliva, M., Salvà-Catarineu, M. (Eds.), *Avances, métodos y técnicas en el estudio del periglacialismo*. Publicacions i Edicions de la Universitat de Barcelona, Barcelona, pp. 323–331.
- Oliva, M., Gómez-Ortiz, A., Palacios, D., Salvador-Franch, F., Andrés, N., Tanarro, L.M., Fernández-Fernández, J.M., Barriocanal, C., 2020. Multiproxy reconstruction of Holocene glaciers in Sierra Nevada (south Spain). *Mediterranean Geoscience Reviews* 1–15. <https://doi.org/10.1007/s42990-019-00008-2>.
- Oskin, M., Burbank, D.W., 2005. Alpine landscape evolution dominated by cirque retreat. *Geology* 33 (12), 933–936. <https://doi.org/10.1130/G21957.1>.
- Paasche, Ø., Dahl, S.O., Bakke, J., Løvlie, R., Nesje, A., 2007. Cirque glacier activity in arctic Norway during the last deglaciation. *Quat. Res.* 68 (3), 387–399. <https://doi.org/10.1016/j.yqres.2007.07.006>.
- Palacios, D., Marcos, J., Vázquez-Selem, L., 2011. Last glacial maximum and deglaciation of Sierra de Gredos, central iberian peninsula. *Quat. Int.* 233, 16–26. <https://doi.org/10.1016/j.quaint.2010.04.029>.
- Palacios, D., de Andrés, N., de Marcos, J., Vázquez-Selem, L., 2012a. Glacial landforms and their palaeoclimatic significance in Sierra de Guadarrama, central iberian peninsula. *Geomorphology* 139–140, 67–78. <https://doi.org/10.1016/j.geomorph.2011.10.003>.
- Palacios, D., Andrés, N., Marcos, J., Vázquez-Selem, L., 2012b. Maximum glacial advance and deglaciation of the Pinar Valley (Sierra de Gredos, Central Spain) and its significance in the Mediterranean context. *Geomorphology* 177–178, 51–61. <https://doi.org/10.1016/j.geomorph.2012.07.013>.
- Palacios, D., Gómez-Ortiz, A., Andrés, N., Salvador, F., Oliva, M., 2016. A Timing and new geomorphological evidence of the last deglaciation stages in Sierra Nevada (southern Spain). *Quat. Sci. Rev.* 150, 110–129. <https://doi.org/10.1016/j.quascirev.2016.08.012>.
- Palacios, D., García-Ruiz, J.M., Andrés, N., Schimmelpenninck, I., Campos, N., Leanni, L., Aster, Team, 2017a. Deglaciation in the central Pyrenees during the Pleistocene-Holocene transition: timing and geomorphological significance. *Quat. Sci. Rev.* 162, 111–127. <https://doi.org/10.1016/j.quascirev.2017.03.007>.
- Palacios, D., Andrés, N., Gómez-Ortiz, A., García-Ruiz, G., 2017b. Evidence of glacial activity during the oldest Dryas in the mountain of Spain. In: Hughes, P., Woodward, J. (Eds.), *Quaternary Glaciation in the Mediterranean Mountains*, vol. 433. Geological Society of London, Special Publication, pp. 87–110. <https://doi.org/10.1144/SP433.10>.
- Palacios, D., Gómez-Ortiz, A., Alcalá-Reygosa, J., Andrés, N., Oliva, M., Tanarro, L., Salvador-Franch, F., Schimmelpenninck, I., Fernández-Fernández, J.M., Léanni, L., 2019. The challenging application of cosmogenic dating methods in residual glacial landforms: the case of Sierra Nevada (Spain). *Geomorphology* 325, 103–118. <https://doi.org/10.1016/j.geomorph.2018.10.006>.
- Pallás, R., Rodés, A., Braucher, R., Carcaillet, J., Ortuño, M., Bordonau, J., Bourlès, D., Vilaplana, J.M., Masana, E., Santanach, P., 2006. Late Pleistocene and Holocene glaciation in the Pyrenees: a critical review and new evidence from ^{10}Be exposure ages, south-central Pyrenees. *Quat. Sci. Rev.* 25, 2937–2963. <https://doi.org/10.1016/j.quascirev.2006.04.004>.
- Pallás, R., Rodés, A., Braucher, R., Bourlès, D., Delmas, M., Calvet, M., Gunnell, Y., 2010. Small, isolated glacial catchments as priority targets for cosmogenic surface exposure dating of Pleistocene climate fluctuations, southeastern Pyrenees. *Geology* 38 (10), 891–894. <https://doi.org/10.1130/G31164.1>.
- Palma, P., Oliva, M., García-Hernández, C., Ortiz, A.G., Ruiz-Fernández, J., Salvador-Franch, F., Catarineu, J.M., 2017. Spatial characterization of glacial and periglacial landforms in the highlands of Sierra Nevada (Spain). *Sci. Total Environ.* 584, 1256–1267. <https://doi.org/10.1016/j.scitotenv.2017.01.196>.
- Rasmussen, S.O., Bigler, M., Blockley, S.P., Blunier, T., Buchardt, S.L., Clausen, H.B., Cvijanovic, I., Dahl-Jensen, D., Johnsen, S.J., Fischer, H., Gkinis, V., Guillevic, M., Hoek, W.Z., Lowe, J.J., Pedro, J.B., Popp, T., Seierstad, I.K., Steffensen, J.P., Svensson, A.M., Vallenga, P., Vinther, B.M., Walker, M.J.C., Wheatley, J.J., Winstrup, M., 2014. A stratigraphic framework for abrupt climatic changes during the Last Glacial period based on three synchronized Greenland ice-core records: refining and extending the INTIMATE event stratigraphy. *Quat. Sci. Rev.* 106, 14–28. <https://doi.org/10.1016/j.quascirev.2014.09.007>.
- Renssen, H., Seppä, H., Heiri, O., Rothe, D.M., Goosse, H., Fichefet, T., 2009. The spatial and temporal complexity of the Holocene thermal maximum. *Nat. Geosci.* 2 (6), 411. <https://doi.org/10.1038/NGEO513>.
- Ribolini, A., Chelli, A., Guglielmin, M., Pappalardo, M., 2007. Relationships between glacier and Rock glacier in the maritime Alps, schiantala valley, Italy. *Quat. Res.* 68, 353–363. <https://doi.org/10.1016/j.yqres.2007.08.004>.
- Rodríguez-Rodríguez, L., Jiménez-Sánchez, M., Domínguez-Cuesta, M.J., Rinterknecht, V., Pallas, R., Bourlès, D., 2016. Chronology of glaciations in the cantabrian mountains (NW Iberia) during the last glacial cycle based on in situ-produced ^{10}Be . *Quat. Sci. Rev.* 138, 31–48. <https://doi.org/10.1016/j.quascirev.2016.02.027>.
- Rodríguez-Rodríguez, L., Jiménez-Sánchez, M., Domínguez-Cuesta, M.J., Rinterknecht, V., Pallas, R., Aster Team, 2017. Timing of last deglaciation in the Cantabrian Mountains (Iberian Peninsula; North Atlantic region) based on in situ-produced ^{10}Be exposure dating. *Quat. Sci. Rev.* 171, 166–181. <https://doi.org/10.1016/j.quascirev.2017.07.012>.
- Sanders, J.W., Cuffey, K.M., Moore, J.R., MacGregor, K.R., Kavanaugh, J.L., 2012. Periglacial weathering and headwall erosion in cirque glacial bergschrunds. *Geology* 40 (9), 779–782. <https://doi.org/10.1130/G33330.1>.
- Sanders, J.W., Cuffey, K.M., MacGregor, K.R., Collins, B.D., 2013. The sediment budget

- of an alpine cirque. *Geol. Soc. Am. Bull.* 125, 229–248. <https://doi.org/10.1130/B30688.1>.
- Sarıkaya, M.A., Çiner, A., Yıldırım, C., 2017. Cosmogenic ^{36}Cl glacial chronologies of the late quaternary glaciers on mount geyikdağ in the eastern mediterranean. *Quat. Geochronol.* 39, 189–204. <https://doi.org/10.1016/j.quageo.2017.03.003>.
- Serrano, E., Oliva, M., González-García, M., López-Moreno, J.I., González-Trueba, J., Martín-Moreno, R., Gómez-Lende, M., Martín-Díaz, J., Nofre, J., Palma, P., 2018. Post-little ice age paraglacial processes and landforms in the high Iberian mountains: a review. *Land Degrad. Dev.* 29, 4186–4208. <https://doi.org/10.1002/ldr.3171>.
- Styllas, M.N., Schimmelpfennig, I., Benedetti, L., Ghilardi, M., Aumaître, G., Bourlès, D., Keddadouche, K., 2018. Late-glacial and Holocene history of the northeast Mediterranean mountain glaciers-New insights from in situ-produced ^{36}Cl -based cosmic ray exposure dating of palaeo-glacier deposits on Mount Olympus, Greece. *Quat. Sci. Rev.* 193, 244–265. <https://doi.org/10.1016/j.quascirev.2018.06.020>.
- Tanarro, L.M., Fernández, J.M., Andres, N., Zamorano, J.J., Sæmundsson, Þ., Brynjólfsson, S., Palacios, D., 2019. Unchanged surface morphology of debris-covered glacier and rock glaciers in Tröllaskagi Peninsula (Northern Iceland). *Sci. Total Environ.* 648, 218–235. <https://doi.org/10.1016/j.scitotenv.2018.07.460>.
- Tomkins, M.D., Dortch, J.M., Hughes, P.D., Huck, J.J., Stimson, A.G., Delmas, M., et al., 2018. Rapid age assessment of glacial landforms in the Pyrenees using Schmidt hammer exposure dating (SHED). *Quat. Res.* 90 (1), 26–37. <https://doi.org/10.1017/qua.2018.12>.
- Uppala, S.M., Kållberg, P., Simmons, A., Andrae, U., Bechtold, V., Fiorino, M., Gibson, J., Woollen, J., 2005. The ERA-40 reanalysis. *Q. J. R. Meteorol. Soc.* 131, 2961–3012. <https://doi.org/10.1256/qj.04.176>.
- Walker, M., Johnsen, S., Rasmussen, S.O., Popp, T., Steffensen, J.P., Gibbard, P., et al., 2009. Formal definition and dating of the GSSP (Global Stratotype Section and Point) for the base of the Holocene using the Greenland NGRIP ice core, and selected auxiliary records. *J. Quat. Sci.* 24 (1), 3–17. <https://doi.org/10.1002/jqs.1227>.
- Zahno, C., Akçar, N., Yavuz, V., Kubik, P.W., Schlüchter, C., 2010. Chronology of late pleistocene glacier variations at the uludağ mountain, NW Turkey. *Quat. Sci. Rev.* 29 (9–10), 1173–1187. <https://doi.org/10.1016/j.quascirev.2010.01.012>.
- Zasadni, J., Klapysa, P., Broś, E., Ivy-Ochs, S., Świąder, A., Christl, M., Balázovičová, L., 2020. Latest Pleistocene glacier advances and post-Younger Dryas rock glacier stabilization in the Mt. Kriváň group, High Tatra Mountains, Slovakia. *Geomorphology* 107093. <https://doi.org/10.1016/j.geomorph.2020.107093>.
- Žebre, M., Sarıkaya, M.A., Stepišnik, U., Yıldırım, C., Çiner, A., 2019. First ^{36}Cl cosmogenic moraine geochronology of the Dinaric mountain karst: velež and Crvanj Mountains of Bosnia and Herzegovina. *Quat. Sci. Rev.* 208, 54–75. <https://doi.org/10.1016/j.quascirev.2019.02.002>.